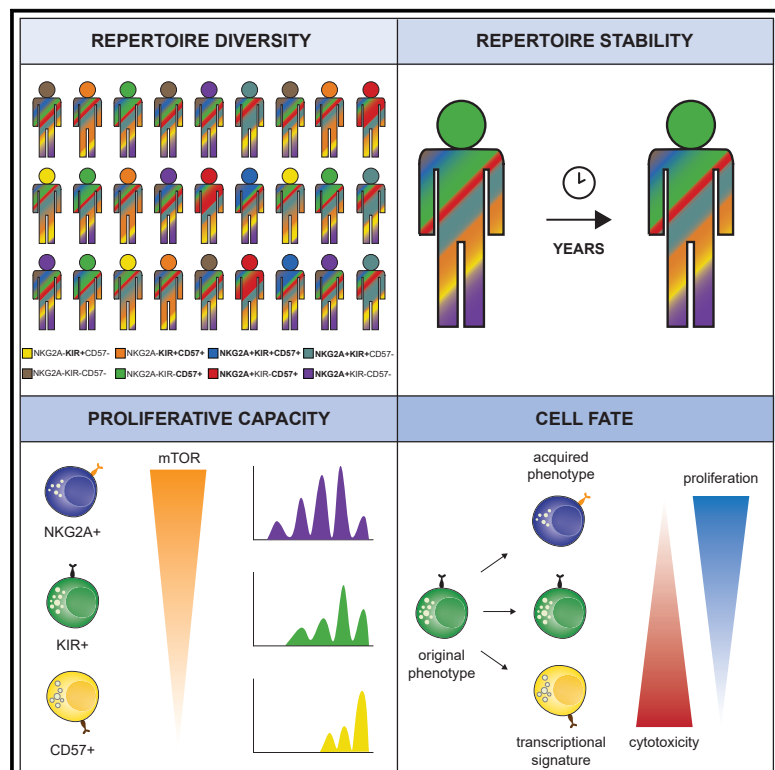


# Intra-lineage Plasticity and Functional Reprogramming Maintain Natural Killer Cell Repertoire Diversity

## Graphical Abstract



## Authors

Aline Pfefferle, Benedikt Jacobs,  
Herman Netskar, ..., Jodie P. Goodridge,  
Ebba Sohlberg, Karl-Johan Malmberg

## Correspondence

kalle.malmberg@ki.se

## In Brief

Unique and genetically hard-wired NK cell repertoires are well-maintained over time despite the rapid turnover of NK cells. Pfefferle et al. identify the role of intra-lineage plasticity during NK cell homeostasis and suggest that a cell's functional fate is tightly linked to its acquired phenotype as determined by transcriptional reprogramming.

## Highlights

- mTOR-dependent hierarchy determines proliferative capacity of NK cells
- NK cell education is an inheritable state during cell division
- Intra-lineage plasticity maintains phenotypic and functional NK cell homeostasis
- The acquired phenotype determines functional potential in NK cells



# Intra-lineage Plasticity and Functional Reprogramming Maintain Natural Killer Cell Repertoire Diversity

Aline Pfefferle,<sup>1</sup> Benedikt Jacobs,<sup>2,3</sup> Herman Netskar,<sup>2,3</sup> Eivind Heggernes Ask,<sup>2,3</sup> Susanne Lorenz,<sup>4</sup> Trevor Clancy,<sup>2,3</sup> Jodie P. Goodridge,<sup>2,5</sup> Ebba Sohlberg,<sup>1</sup> and Karl-Johan Malmberg<sup>1,2,3,6,\*</sup>

<sup>1</sup>Center for Infectious Medicine, Department of Medicine Huddinge, Karolinska Institutet, Stockholm, Sweden

<sup>2</sup>Department of Cancer Immunology, Institute for Cancer Research, Oslo University Hospital, Oslo, Norway

<sup>3</sup>The KG Jebsen Center for Cancer Immunotherapy, Institute of Clinical Medicine, University of Oslo, Oslo, Norway

<sup>4</sup>Department of Tumor Biology, Institute for Cancer Research, Oslo University Hospital, Oslo, Norway

<sup>5</sup>Fate Therapeutics, Inc., San Diego, CA, USA

<sup>6</sup>Lead Contact

\*Correspondence: kalle.malmberg@ki.se

<https://doi.org/10.1016/j.celrep.2019.10.058>

## SUMMARY

Natural killer (NK) cell repertoires are made up of phenotypically distinct subsets with different functional properties. The molecular programs involved in maintaining NK cell repertoire diversity under homeostatic conditions remain elusive. Here, we show that subset-specific NK cell proliferation kinetics correlate with mTOR activation, and global repertoire diversity is maintained through a high degree of intra-lineage subset plasticity during interleukin (IL)-15-driven homeostatic proliferation *in vitro*. Slowly cycling sorted KIR<sup>+</sup>CD56<sup>dim</sup> NK cells with an induced CD57 phenotype display increased functional potential associated with increased transcription of genes involved in adhesion and immune synapse formation. Rapidly cycling cells upregulate NKG2A, display a general loss of functionality, and a transcriptional signature associated with increased apoptosis/cellular stress, actin-remodeling, and nuclear factor κB (NF-κB) activation. These results shed light on the role of intra-lineage plasticity during NK cell homeostasis and suggest that the functional fate of the cell is tightly linked to the acquired phenotype and transcriptional reprogramming.

## INTRODUCTION

Since their discovery in the early 1970s, our view of natural killer (NK) cells has developed from a uniform and short-lived cell population to a group of effectors vastly diverse in phenotype, functionality, and lifespan (Vivier et al., 2011). Mapping of NK cell subset diversity by mass cytometry revealed more than 10<sup>5</sup> unique NK cell subsets (Horowitz et al., 2013). Stochastic expression of killer cell immunoglobulin-like receptors (KIRs) and heterogeneously expressed activating/inhibitory receptors contribute to the intra/inter-donor diversity of the NK cell repertoire (Cichocki et al., 2014).

The NK cell differentiation spectrum spans from less differentiated CD56<sup>bright</sup> cells to terminally differentiated adaptive CD56<sup>dim</sup> cells (Foley et al., 2012; Poli et al., 2009; Sun et al., 2009). Immunoregulatory CD56<sup>bright</sup> NK cells are highly responsive to cytokines while cytotoxic CD56<sup>dim</sup> NK cells favor receptor ligation input (Goodridge et al., 2015). A maturation spectrum, defined by HLA-binding NKG2A and KIR and the terminal differentiation marker CD57, further differentiates the functionally diverse CD56<sup>dim</sup> subset (Björkström et al., 2010). Adaptive NK cells, identified in ~40% of cytomegalovirus (CMV) seropositive individuals, are a terminally differentiated NK cell subset, the generation of which is accelerated by CMV (Béziat et al., 2013; Della Chiesa et al., 2012; Foley et al., 2012; Gumá et al., 2004; Lopez-Vergès et al., 2011; Schlums et al., 2015). These cells exhibit heightened cytotoxic capacity and increased longevity and thus represent a subset of great interest to adoptive cell therapy (Liu et al., 2015).

Although no strict maturation scheme exists, phenotyping based on NKG2A, KIR, and CD57 expression has served as a useful tool for grouping NK cells based on functional, metabolic, and proliferative ability, as well as their longevity (Goodridge et al., 2015; Liu et al., 2015). Mouse studies identified critical roles for T-bet and Eomes in the transition from CD27<sup>+</sup>CD11b<sup>-</sup> to CD27<sup>-</sup>CD11b<sup>+</sup> cells, but the intracellular signaling pathways activating these transcription factors are still not understood (Gordon et al., 2012; Ranson et al., 2003b). Collins et al. (2019) recently identified subset specific transcriptional regulators between CD56<sup>bright</sup> and CD56<sup>dim</sup> NK cells. However, the molecular programs involved in maintaining NK cell repertoire diversity under homeostatic conditions remain elusive.

Interleukin (IL)-15 is the main homeostatic NK cell cytokine due to its vital role in survival, development, and proliferation (Anton et al., 2015; Ranson et al., 2003a, 2003b). IL-15 signals via JAK1/3 activating the transcription factor STAT5, but can also activate the mammalian target of rapamycin (mTOR) in a dose-dependent manner (Marçais et al., 2014). This serine/threonine kinase can form two protein complexes: mTOR complex 1 (mTORC1) senses nutrients in the microenvironment and via metabolic reprogramming can control the cell's metabolism, while mTOR complex 2 (mTORC2) aids in controlling the cell's cytoskeletal



organization (Donnelly et al., 2014). In murine NK cells, mTORC1 activation mediated increased effector function by shifting from predominantly oxidative phosphorylation to glycolysis (Donnelly et al., 2014; Keating et al., 2016; Nandagopal et al., 2014; Viel et al., 2016). Although mTORC1 activation sustains mTORC2, using a negative feedback loop, mTORC2 can suppress mTORC1 induced effector functions in mice (Wang et al., 2018). In humans, mTOR's role in maintaining homeostasis requires further investigation.

Within individuals, the diverse and unique NK cell pool is well-maintained over time (Béziat et al., 2013). This stability in receptor repertoires combined with the rapid turnover of NK cells (Lutz et al., 2011) hints at the important role proliferation plays in replenishing the NK cell pool at steady state. The question arises if this observed stability during homeostatic proliferation is the result of self-renewal from an immature pool of progenitor cells followed by differentiation or arises due to plasticity within the NK cell subsets.

Intra-lineage cell plasticity, also known as functional plasticity, is the term describing phenotypic and functional changes occurring within a given cell lineage (Laurent et al., 2017). Functional plasticity is an adaptation of the immune system to its surroundings, such as the M1-M2 transition in macrophages, the T<sub>h</sub>-T<sub>reg</sub> transition in T cells, and the transition between innate lymphoid cell (ILC) subsets. Functional plasticity is the result of cytokine or receptor input and is translated into transcriptional changes resulting in modified functionality (Colonna, 2018). NK cell plasticity has largely been unexplored, with the exception of transforming growth factor  $\beta$  (TGF- $\beta$ )-induced NK cell conversion into intermediate ILC1-like cells (Gao et al., 2017).

Based on their cytotoxic capacity and ability to direct the adaptive immune response through cytokine secretion and interactions with antigen presenting cells, T cells and B cells, NK cells hold great potential in the clinic as a cancer treatment. This is made evident by the numerous clinical trials currently being evaluated. To fully harness the clinical potential of NK cells, we need to further our understanding of the vast repertoire diversity and the fundamental mechanisms governing the intrinsic functional potential of distinct NK cell subsets at steady state and following cytokine stimulation.

In this study, we show that NK cell repertoire diversity is maintained during IL-15-driven homeostatic proliferation through a combination of mTOR-dependent hierarchy in proliferation capacity and a substantial degree of intra-lineage plasticity. Subset plasticity at the phenotypic level is tightly linked to the functional fate of the cell and associated with upregulation of distinct transcriptional programs that define the acquired phenotype. These results provide insights into the cellular and molecular programs involved in regulating NK cell homeostasis at the single-cell level.

## RESULTS

### Subset-Specific Proliferation Kinetics

We set out to study the cellular and molecular events associated with the shift from a quiescent to a proliferative state during homeostatic proliferation in NK cells. To this end, we stimulated purified primary human NK cells with 5 ng/mL of IL-15 daily, monitored the onset of proliferation and tracked subsequent

cell divisions using a proliferation dye. At the population level, cell division commenced on day 3 along a linear path (Figures 1A and 1B). Slight inter-donor variations in proliferation and subset distribution were observed (Figure S1). We have previously identified a hierarchy in the proliferative response determined by NK cell differentiation defined through expression patterns of NKG2A, KIR, and CD57 (Björkström et al., 2010). Therefore, we stratified the analysis of NK cell proliferation kinetics according to differentiation status into 8 distinct subsets based on the expression of NKG2A, KIR, and CD57. CD57 expression had the strongest impact on proliferation speed, resulting in a slightly delayed onset, slower subsequent cell divisions, and a low proliferation index (Figures 1C and 1D). Notably, NKG2A<sup>-</sup>KIR<sup>+</sup> NK cells proliferated more slowly than NKG2A<sup>-</sup>KIR<sup>-</sup> NK cells, independent of CD57 expression (Figures 1C and 1D). We have previously shown that proliferation is uncoupled from education (Björkström et al., 2010), and the reduced proliferative response in KIR<sup>+</sup> cells is therefore most likely a result of differentiation and reduced cytokine responsiveness. Importantly, however, irrespective of subset-specific differences in proliferation kinetics, the global NK cell repertoires remained largely stable during the one-week time frame in this experimental set up (Figure 1E). Thus, this *in vitro* model allowed us to tease apart subset-specific behavior under conditions that mimic natural NK cell repertoire homeostasis.

### mTOR Activation Determines Proliferation Kinetics

Given that mTOR has been implicated in NK cell proliferation (Marçais et al., 2014), we first examined the relationship between mTOR activation and proliferation kinetics. A downstream target of mTORC1 is the ribosomal protein S6 (pS6) that becomes phosphorylated upon mTORC1 activation (Marçais et al., 2014). pS6 expression increased with subsequent cell divisions in cycling cells (day 5) (Figures 2A and 2B) and mTORC1 inhibition led to decreased pS6 and Ki-67 levels (Figures S2A and S2B). Prior to cell division (day 2), donor-specific pS6 upregulation was noted and positively correlated with subsequent cell division (day 3) (Figure 2C). Furthermore, early pS6 upregulation (day 2) could function as a predictive marker for donor-specific proliferation potential (day 5) (Figure 2D).

Next, we sampled the same individuals monthly over a three-month period. IL-15-induced pS6 induction varied greatly among subsets (Figure 2E), prompting further analysis of the role subset distribution plays in determining donor proliferation kinetics. The percentage of NKG2A<sup>+</sup>KIR<sup>-</sup>CD57<sup>-</sup> and NKG2A<sup>-</sup>KIR<sup>-</sup>CD57<sup>+</sup> cells at baseline correlated positively or negatively, respectively, with pS6 fold change at the donor level (day 2) (Figure 2F) and with proliferation on day 5 (Figure 2G). Furthermore, these parameters were stable within donors over the three-month period (Figures 2F and 2G). Hence, at the donor level subset distribution correlated with overall pS6 upregulation and proliferation potential.

NKG2A<sup>+</sup>KIR<sup>-</sup>CD57<sup>-</sup> cells exhibited the highest fold change and inter-donor variation in pS6 expression (Figure 2E), where early upregulation again correlated with subsequent proliferation (Figure 2H). Therefore, the donor variation in proliferative capacity at a global level is determined in part by the subset composition at baseline and in part by a donor-dependent metabolic set

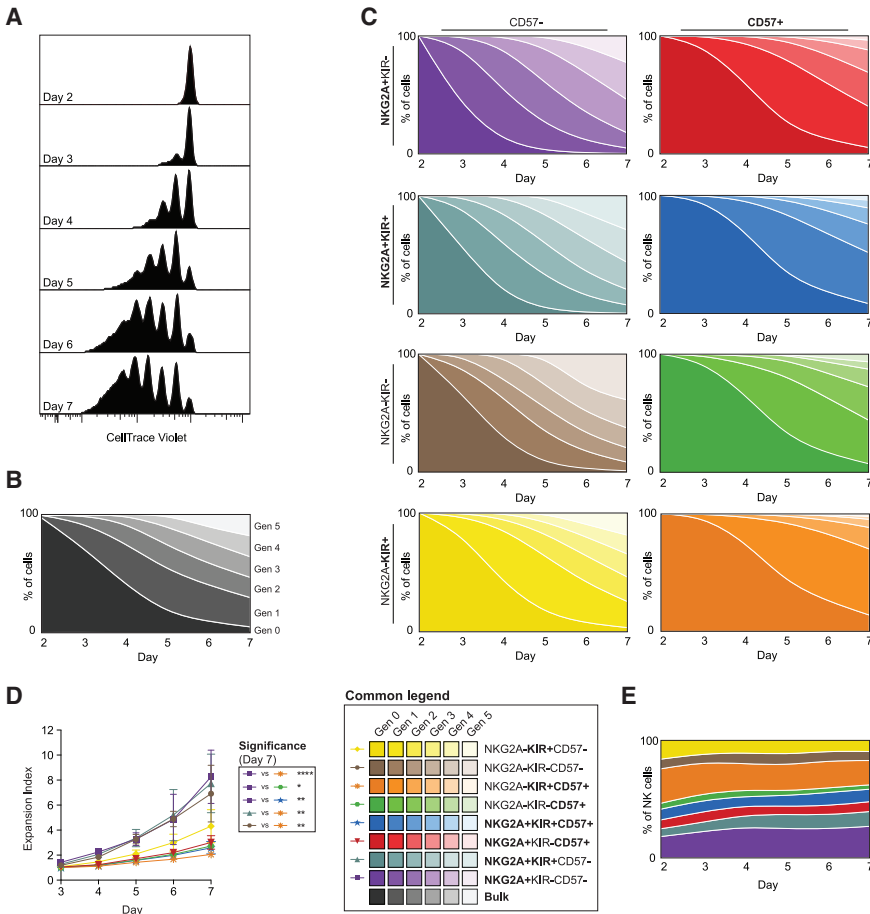


**Figure 1. Proliferation Kinetics of Freshly Isolated Human NK Cell Subsets**

(A) Cell division as measured by CellTrace violet (CTV) dilution for the total CD56<sup>+</sup> NK cell population from days 2–7 of a representative donor. Each peak represents one generation.

(B and C) Visual representation of the proliferation kinetics of the total CD56<sup>+</sup> NK cell population (B) and of 8 subsets (defined by Boolean gating of NKG2A, KIR, and CD57 expression) (C) in donors from days 2–7.

(D and E) Expansion index (D) and visualization of the same 8 subset frequencies (E) that together comprise the total NK cell population from days 2–7. n = 6.

Data are represented as mean (SD) and from one representative experiment. Significance was calculated using a Friedman test followed by Dunn's multiple comparisons test (D). \*p < 0.05, \*\*p < 0.01, \*\*\*p < 0.001, \*\*\*\*p < 0.0001.

See also Figure S1.

level (Figure S3). The population map showed a clear distinction between slowly (generation 0–1) and rapidly cycling (generation 2+) cells (Figure S3). Stratifying the NKG2A-KIR-CD57<sup>-</sup> sorted cells based on proliferation, highlighted the impact proliferation kinetics have on the acquired phenotype. High proliferation rate was associated with NKG2A expression and slow proliferation rate with CD57 expression, both at the subset (Figure 3C) and population level (Figure S3). Although proliferation

impacted the acquired phenotype, the degree of plasticity was proliferation-independent, as the size of the original phenotypic subset (NKG2A-KIR<sup>+</sup>CD57<sup>-</sup>) was similar in both groups on day 6 (Figure 3C).

Thus, IL-15-induced plasticity was evident in NK cells across the differentiation spectrum and contributed to the maintenance of repertoire diversity at the population level.

### The Acquired Phenotype Determines Functional Responses

As NK cell differentiation is associated with changes in functional potential (Liu et al., 2015), acquisition of differentiation markers may have functional consequences. Acquisition of NKG2A expression in sorted NKG2A-KIR-CD57<sup>-</sup> cells resulted in a significantly higher expansion index (Figure 4A), while CD57 acquisition resulted in increased degranulation and cytokine production post target cell stimulation (Figures 4B and 4C). Fluorescence-activated cell sorting (FACS) sorted slowly cycling cells, exhibiting a higher proportion of CD57<sup>+</sup> cells, displayed higher killing capacity compared to rapidly cycling, predominantly NKG2A<sup>+</sup> NK cells (Figures 4D and 4E), further validating the functional consequences of phenotypic modifications.

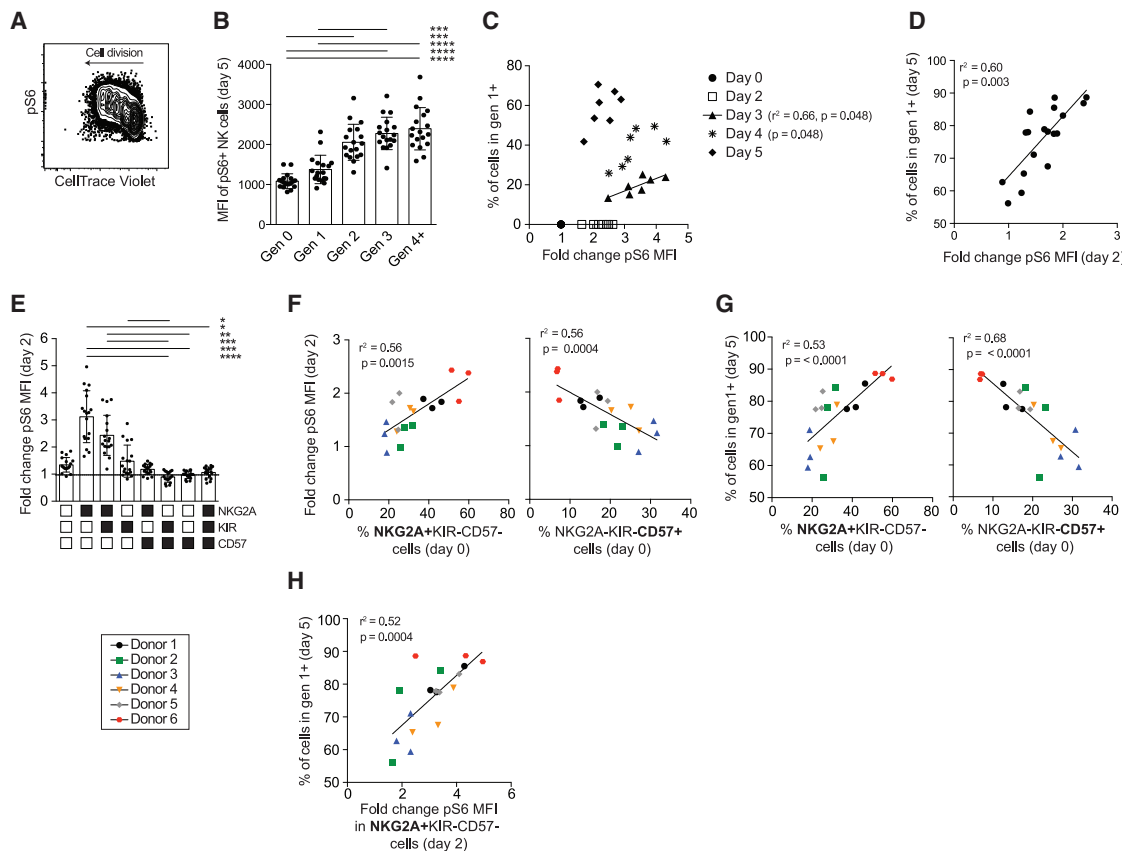
In NK cells, the functional potential is tuned by a process termed education, where interactions between self-MHC class

point determining the level of mTOR activation in response to IL-15 stimulation.

### IL-15-Induced Intra-lineage Plasticity

Subset frequencies were largely retained at the population level (Figure 1E), irrespective of subset-specific proliferation kinetics (Figure 1D), warranting the investigation of IL-15-induced intra-lineage plasticity. We monitored phenotypic changes in sorted NK cell subsets at distinct stages of differentiation (NKG2A<sup>+</sup>KIR<sup>-</sup>CD57<sup>-</sup>, NKG2A<sup>-</sup>KIR<sup>+</sup>CD57<sup>-</sup>, NKG2A<sup>-</sup>KIR<sup>-</sup>CD57<sup>+</sup>, NKG2A<sup>-</sup>selfKIR<sup>+</sup>CD57<sup>+</sup>NKG2C<sup>+</sup>) after IL-15 stimulation (Figure 3A). After 6 days, a remarkable amount of plasticity was observed, particularly in the NKG2A<sup>-</sup>KIR<sup>+</sup>CD57<sup>-</sup> subset (Figure 3B). Acquisition of NKG2A or CD57 was most common, with KIR2DL1 or KIR2DL3 acquisition being less frequent (Figure 3B), possibly due to the well-established role of promoter methylation in determining KIR expression (Santourlidis et al., 2002). Although NKG2A acquisition was also observed in sorted adaptive NK cells, these cells exhibited higher phenotypic stability illustrated by the uniform retention of CD57 expression.

To determine if the observed plasticity was dependent on the degree of proliferation, we used t-Distributed Stochastic Neighbor Embedding (t-SNE) analysis to visualize the phenotypic consequences of IL-15-driven plasticity at the generation

**Figure 2.** mTOR Activation Correlates with NK Cell Proliferation Kinetics

(A and B) Representative FACS plot showing pS6 expression in each generation after 5 days of IL-15 stimulation as visualized by CTV dilution (A) and summary of results (B).

(C) Fold change in pS6 MFI plotted against the frequency of cells having divided at least once (generation 1+) at baseline (day 0) and on days 2–5.

(D) Fold change in pS6 MFI on day 2 prior to the onset of proliferation, plotted against the frequency of cells proliferating (generation 1+) on day 5.

(E) Fold change in pS6 MFI on day 2 within 8 NK cell subsets.

(F and G) Frequency of two subsets ( $\text{NKG2A}^+\text{KIR}^-\text{CD57}^-$  and  $\text{NKG2A}^-\text{KIR}^-\text{CD57}^+$ ) at baseline plotted against the fold change in pS6 MFI on day 2 for the total NK cell population (F) or the total frequency of cells proliferating (generation 1+) on day 5 (G).

(H) Fold change in pS6 MFI within  $\text{NKG2A}^+\text{KIR}^-\text{CD57}^-$  cells on day 2 versus the total frequency of cells proliferating (generation 1+) on day 5.

In (F)–(H), each color denotes the same donor sampled monthly over a three-month interval.  $n = 7\text{--}18$ . Data are represented as mean (SD) and from 5 independent experiments. Significance was calculated using a Friedman test followed by a Dunn's multiple comparisons test (B), (E), or a Spearman r test (C, D, and F–H).

\* $p < 0.05$ , \*\* $p < 0.01$ , \*\*\* $p < 0.001$ , \*\*\*\* $p < 0.0001$ .

See also Figure S2.

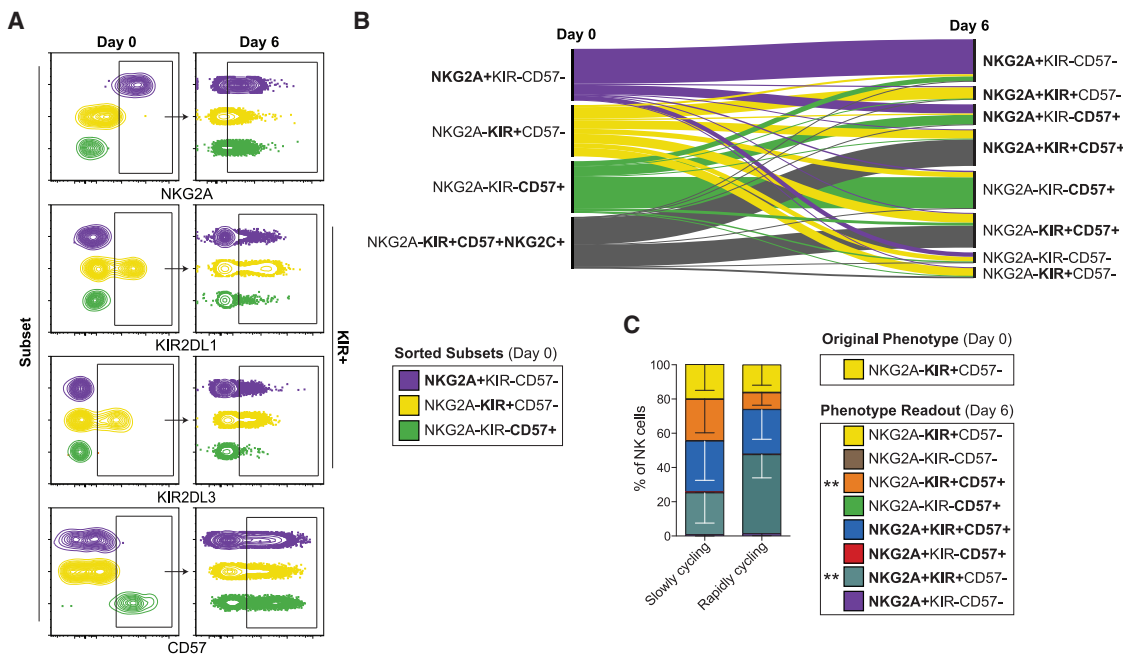
I ligands and inhibitory receptors are translated into increased effector potential (Goodridge et al., 2015). t-SNE analysis of inhibitory KIRs revealed a narrower repertoire in rapidly cycling cells compared to slowly cycling cells expressing multiple KIRs (Figures S4A and S4B). The education status, determined by the level of degranulation in self and non-self KIR<sup>+</sup> NK cells in response to target cell stimulation, was inherited in rapidly cycling cells albeit less pronounced compared to slowly cycling cells (Figure 4F).

These data demonstrate that decreased functionality in rapidly cycling NK cells was mainly related to an induced less differentiated NKG2A<sup>+</sup> phenotype compared to the more differentiated CD57<sup>+</sup> phenotype induced in slowly cycling cells. Hence, the cell's acquired phenotype, and not its origin, determined its functional capabilities in terms of cytotoxicity and proliferation.

### IL-15-Induced Transcriptional Reprogramming

To identify transcriptional programs associated with intra-lineage plasticity, we performed single-cell RNA sequencing. Sorted NKG2A<sup>-</sup>selfKIR<sup>+</sup>CD57<sup>-</sup> NK cells were cultured with IL-15 for 6 days to induce plasticity and then sorted into slowly and rapidly cycling cells prior to sequencing (Figures S5A–S5C). Additionally, two functionally diverse subsets, less differentiated ( $\text{NKG2A}^+\text{KIR}^-\text{CD57}^-$ ) and more differentiated ( $\text{NKG2A}^-\text{selfKIR}^+\text{CD57}^+$ / $\text{NKG2A}^+\text{selfKIR}^+\text{CD57}^+\text{NKG2C}^+$ ), were sorted and sequenced at baseline (Figures S5A and S5B).

Uniform manifold approximation and projection (UMAP) embedding of the four day-6 samples (7,207 cells), after data integration with Seurat 3.0 (Hafemeister and Satija, 2019; Stuart et al., 2018) to eliminate donor-dependent variation, revealed that the transcriptomes separated mostly based on the rate

**Figure 3. IL-15-Induced NK Cell Intra-lineage Plasticity**

(A and B) Representative FACS plot of phenotypic markers (NKG2A, KIR2DL1, KIR2DL3, CD57) used for FACS sorting of three subsets in a non-adaptive donor on day 0 and the expression of those markers on the sorted subsets after 6 days of IL-15-induced proliferation (A) and visualization of the results (B).

(C) Distribution of 8 subset frequencies in previously sorted NKG2A<sup>-</sup>KIR<sup>+</sup>CD57<sup>-</sup> cells further stratified into slowly (generation 0–1) and rapidly cycling (generation 2+) cells after 6 days of culture. n = 11 donors from 5 independent experiments.

Data are represented as mean (SD). Significance of individual subset frequencies between slowly and rapidly cycling cells was calculated using a Wilcoxon signed rank test (C). In (B), two donors with an adaptive phenotype were included. \*\*p < 0.01. Whiskers show SD. See also Figure S3.

of proliferation (Figures S5D and S5E). Given that the majority of the 7,207 cells were actively proliferating at day 6, we also plotted the cell-cycle phase in the same UMAP embedding and focused our downstream analysis on the G1 phase, corresponding to 49% of the cells (3,502 cells) (Figure 5A). We identified 63 differentially expressed genes (DEGs) within the G1 cell-cycle phase between slowly and rapidly cycling cells, with 24 and 39 genes being upregulated in slowly and rapidly cycling cells, respectively (Figures 5B and 5C; Table S1).

To address whether the IL-15-induced subset plasticity was associated with transcriptional reprogramming, we first performed data integration of the four baseline samples to control for variation at the donor level (Figure S5F). Baseline transcriptomes of 7,908 resting NK cells revealed no clustering based on cell-cycle phase (Figure S5F). We next utilized data integration to combine the four baseline samples with the day-6 cells within the G1 cell-cycle phase in order to compare the transcriptional signatures of slowly and rapidly cycling cells with those of defined subsets at baseline (Figure 5D). The cells clustered into two distinct populations, with cluster 1 largely corresponding to slowly cycling (day 6) and more differentiated cells (baseline) whereas cluster 2 largely corresponded to rapidly cycling (day 6) and less differentiated cells (baseline) (Figure 5E).

Using a data imputation method, Markov affinity-based graph imputation of cells (MAGIC), the data were denoised

in order to optimize gene expression analysis on the UMAP embedding (van Dijk et al., 2018). We plotted gene expression of the 63 DEGs between slowly and rapidly cycling cells onto the UMAP embedding of both our baseline and day-6 samples (Figures 5F, 5G, and S5G) (van Dijk et al., 2018). In line with transcriptional reprogramming of the day-6 samples toward the baseline signatures, genes upregulated in slowly cycling cells exhibited higher expression within cluster 1, while genes associated with rapidly cycling cells were generally higher expressed in cluster 2. The transcriptional signature of slowly cycling cells was associated with innateness/quiescence (*LITAF*, *ZFP36L2*), adhesion/immune synapse (*S100A4*, *TIMP1*), as well as increased NK cell differentiation (*FGFBP2*, *FCGR3A*, *PTPRC*) and cytotoxicity (*CCL5*, *KLRF1*, *FCGR3A*) (Figure 5F). Meanwhile the transcriptional signature of rapidly cycling cells was associated with decreased differentiation (*KLRC1*, *GZMK*, *TNFSF10*) and functionality (*ENTPD1*), as well as increased actin-modulating genes (*ASB2*, *CAPG*, *COTL1*), proliferation (*NME1*, *CCND2*, *FBXO6*), apoptosis/cellular stress (*BCL7C*, *CEBPD*, *HSPD1*, *FBXO6*), and NF-κB activation (*ASB2*, *TESC*) (Figure 5G).

Hence, IL-15-driven intra-lineage plasticity and the associated shift in functional responses was associated with transcriptional reprogramming toward the baseline signature of NK cells with the acquired phenotype.

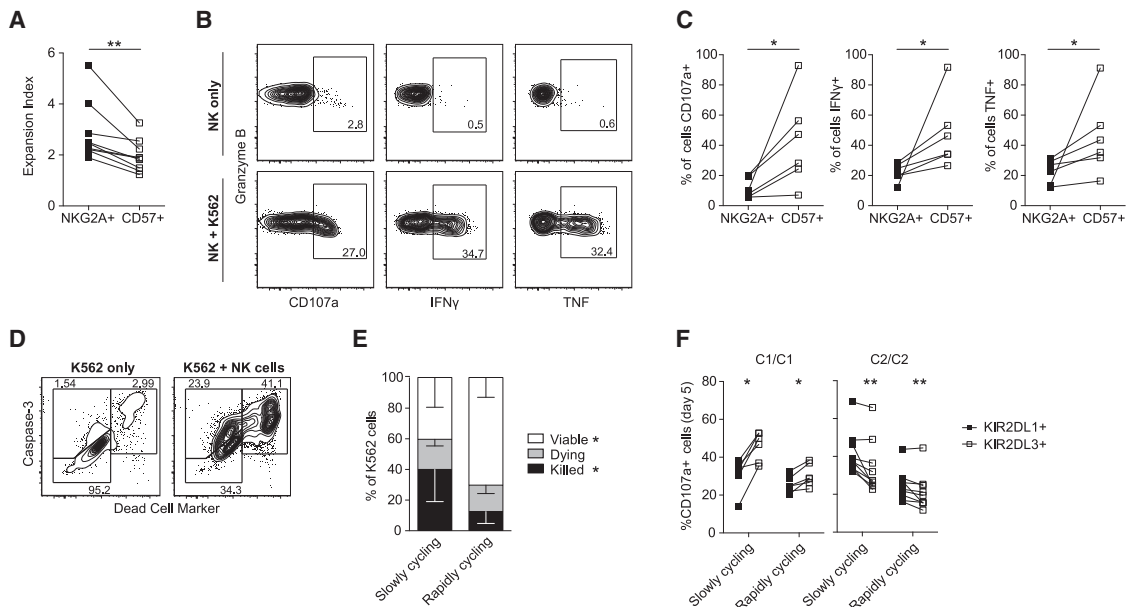


**Figure 4. Proliferative and Functional Consequences of Intra-lineage Plasticity**

(A) Expansion index of sorted NKG2A<sup>-</sup>KIR<sup>+</sup>CD57<sup>-</sup> cells having acquired either NKG2A or CD57 expression on day 6.  
 (B and C) Representative FACS plots of degranulation (CD107a) and cytokine production (IFN $\gamma$ <sup>+</sup>, TNF<sup>+</sup>) in controls (NK only) and in response to K562 cells (NK + K562) (B), and summary of results in sorted NKG2A<sup>-</sup>KIR<sup>+</sup>CD57<sup>-</sup> cells having acquired either NKG2A or CD57 expression on day 6 (C).  
 (D and E) Representative FACS plots of the K562 killing assay, where K562 cells are stratified into viable (caspase 3<sup>-</sup> DCM<sup>-</sup>) and killed (caspase 3<sup>+</sup> DCM<sup>+</sup>) (D), and summary of results for day 5 NK cells FACS sorted into slowly (generation 0–1) and rapidly cycling (generation 2+) cells (E).  
 (F) Frequency of CD107a<sup>+</sup> in single KIR<sup>+</sup> NK cells expressing a self or non-self KIR in C1/C1 or C2/C2 donors divided into slowly (generation 0–1) and rapidly cycling (generation 2+) cells on day 5. n = 6–9 from 9 independent experiments.

Data are represented as mean (SD). Significance between NKG2A<sup>+</sup> and CD57<sup>+</sup> cells (A) and (C), slowly and rapidly cycling cells (E) and KIR2DL1<sup>+</sup> and KIR2DL3<sup>+</sup> cells (F) was calculated using a Wilcoxon signed rank test. \*p < 0.05, \*\*p < 0.01.

See also Figure S4.

## DISCUSSION

IL-15 is a key homeostatic cytokine for NK cells, linked to survival, differentiation, functionality, and proliferation, but how these processes come together to maintain stable and highly diverse repertoires within individuals remains elusive (Ali et al., 2015; Anton et al., 2015; Lin et al., 2017; Marçais et al., 2014; Nandagopal et al., 2014; Zhang et al., 2018). We developed an *in vitro* model to study IL-15-driven homeostasis at the single-cell and repertoire level and noted a striking mTOR-dependent hierarchy in proliferative responses among discrete NK cell subsets. Yet, despite profound subset-specific proliferation kinetics, the global repertoires remained relatively stable suggesting that proliferation differences between subsets could be balanced by plasticity.

Intra-lineage plasticity, the phenotypic and functional changes occurring within a given cell lineage (Laurent et al., 2017), remains largely understudied in the context of NK cells. Most studies published so far have examined dynamic phenotypic changes in the NK cell repertoire in a tumor setting, using mouse models or tumor cell lines (Gao et al., 2017; Streltsova et al., 2018). Here, we observed a high degree of NK cell plasticity across the differentiation spectrum in response to IL-15 stimulation. We focused our analysis on NKG2A<sup>-</sup>KIR<sup>+</sup>CD57<sup>-</sup>CD56<sup>dim</sup> NK cells and followed their phenotypic and functional fate after

IL-15-induced proliferation. At the phenotypic level, we noted a high degree of plasticity dominated by NKG2A or CD57 acquisition along with retained KIR expression. Although terminally differentiated adaptive NK cells exhibited the highest phenotypic stability, possibly due to their epigenetic imprinting (Schlums et al., 2015), activation induced NKG2A acquisition could still be observed. At the functional level, induced NKG2A<sup>+</sup>KIR<sup>+</sup>CD57<sup>-</sup> NK cells displayed strong proliferative responses, whereas induced NKG2A<sup>-</sup>KIR<sup>+</sup>CD57<sup>+</sup> NK cells exhibited increased responsiveness to target cell stimulation.

Maintaining the balance between proliferation and differentiation is an important aspect of normal hematopoiesis, because differentiation arrests at early stages of development can lead to uncontrolled proliferation (Heuzé et al., 2008). Even within well-defined cell lineages, such as T cells, this balance of proliferation versus differentiation/functionality is evident. A detailed comparison between innate and adaptive T cells identified key aspects that defined “innateness” compared to “adaptiveness” (Gutierrez-Arcelus et al., 2019). Innateness was associated with increased functionality, with ribosomes being utilized to translate preformed mRNA allowing for a rapid response. Adaptiveness, meanwhile, was associated with increased proliferation, whereby ribosomes were utilized for ribosome biogenesis to meet energy requirements. This was also associated with increased reactive oxygen species (ROS)

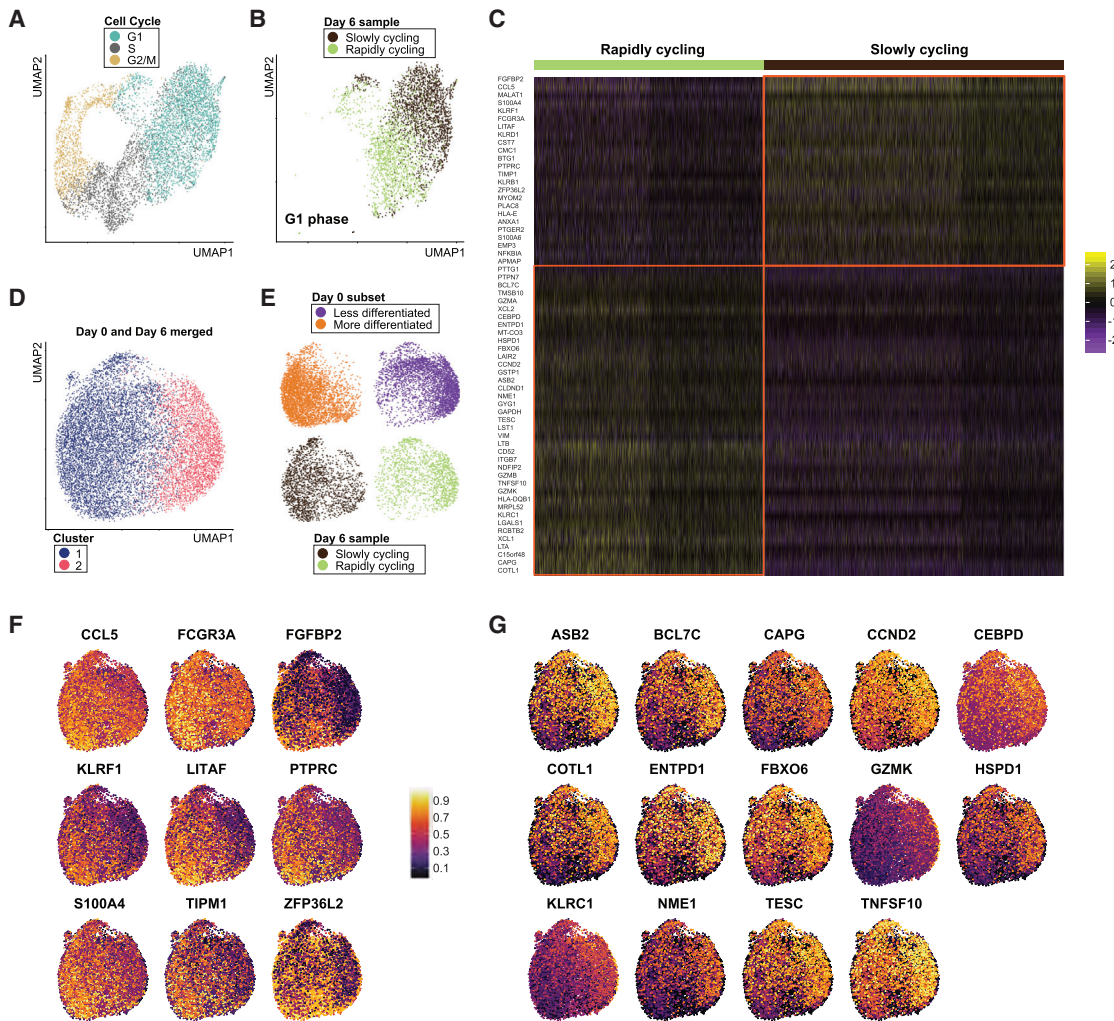


**Figure 5. Transcriptional Signatures of Resting and Proliferating NK Cell Subsets through Single-Cell RNA Sequencing**

(A) UMAP embedding of cell-cycle phases of integrated single-cell RNA sequencing data of FACS-sorted NKG2A<sup>-</sup>selfKIR<sup>+</sup>CD57<sup>-</sup> cells after 6 days of IL-15 stimulation sorted into slowly (generation 0–1) and rapidly cycling (generation 2+) cells from two donors.

(B) UMAP embedding of slowly and rapidly cycling cells within the G1 cell-cycle phase as identified in (A).

(C) Expression heatmap of the 63 differentially expressed genes (DEG) between slowly and rapidly cycling cells within the G1 cell-cycle phase as shown in (B).

(D and E) UMAP embedding of integrated data from two baseline subsets and the IL-15 stimulated (day 6) slowly and rapidly cycling samples in the G1 phase depicting clustering (D) and visualization of the individual samples (E).

(F and G) Imputed gene expression of a selection of the 63 DEGs upregulated in slowly cycling cells (F) and rapidly cycling cells (G) plotted onto the UMAP embedding of the baseline and day 6 samples. n = 4–8 from 4 independent experiments.

See also Figure S5 and Table S1.

levels. Hence, increased effector function is associated with a loss of proliferative capacity in T cells. This is in line with homeostatic proliferation studies in lymphopenic mice that identified phenotypic and functional changes to the T cell repertoire, including a functional inability during the initial phase of proliferation post transfer. Most importantly, complete reversal of phenotypic changes was observed once proliferative cues were eliminated (Boymann et al., 2009; Goldrath et al., 2000; Min, 2018). These studies bear striking similarity with the functional dichotomy between rapid and slowly cycling NK cells, and it would be interesting to determine if rapidly cycling cells could regain functionality in the absence of proliferation cues.

Metabolism, controlled by mTOR, is a key regulatory mechanisms behind immune cell differentiation and function (Soliman, 2013), but the exact signaling cascade remains unknown (Ali et al., 2015; Donnelly et al., 2014; Marçais et al., 2017; Viel et al., 2017; Wang et al., 2018; Yang et al., 2018). Mouse studies have identified an IL-15 stimulation threshold for mTORC1 activation, where suboptimal stimulation only activated STAT5. Similarly, we observed a large variation in mTORC1 activity at the donor and subset level, which could predict the subsequent degree of proliferation. It is possible that polymorphisms in HLA-B ( $\sim$ 21M/T) at the donor level, which has been linked to different education and functional status of

NKG2A expressing NK cells, could further contribute to the donor-specific mTOR activation observed (Horowitz et al., 2016). Less differentiated NKG2A<sup>+</sup> cells are highly responsive to cytokine stimulation (Björkström et al., 2010), and rapidly cycling NKG2A<sup>+</sup> NK cells exhibited the highest pS6 fold change, suggesting that they reached the mTORC1 activation threshold. Hence, mTOR activation may play a role in inducing the less differentiated NKG2A<sup>+</sup>KIR<sup>+</sup>CD57<sup>-</sup> phenotype in cytokine responsive, rapidly cycling cells. These data suggest that the mTOR pathway is most important during early differentiation whereas terminal differentiation may be regulated by other IL-15-induced pathways.

Identification of transcriptional signatures from integrated single-cell RNA sequencing (scRNA-seq) data of 7,908 cells from less and more differentiated subsets at baseline and slowly and rapidly cycling cells at day 6 revealed two main clusters. Cluster 1 consisted of slowly cycling cells and the more differentiated subset at baseline, while rapidly cycling cells clustered together with the less differentiated subset at baseline forming cluster 2. Supporting the phenotypic changes and transcriptional signature, a number of genes associated with NK cell differentiation were differentially expressed between slowly and rapidly cycling cells. *FGFBP2* (Ksp37), *FCGR3A* (CD16), and *PTPRC* (CD45) were upregulated in slowly cycling, while *KLRC1* (NKG2A), *GZMK* (granzyme K), and *TNFSF10* (TRAIL) were upregulated in rapidly cycling. Granzyme K is highly expressed in CD56<sup>bright</sup> NK cells while TRAIL expression is associated with immature NK cells in newborn mice and the adult mouse liver but can also be induced on CD56<sup>bright</sup> NK cells through interferon alpha (IFN $\alpha$ ) stimulation (Stegmann et al., 2010; Takeda et al., 2005). Increased expression of *KRLC1* was in line with NKG2A upregulation at the protein level in rapidly cycling cells. CD45 expression plays an important role in mediating immunoreceptor tyrosine-based activation motif (ITAM)-specific NK cell functions and low CD45 expression is also associated with immature CD56<sup>bright</sup> NK cells (Hesslein et al., 2011; Krzywinska et al., 2016). Hence slowly cycling cells exhibited a transcriptional profile associated with a more differentiated phenotype compared to rapidly cycling cells.

Even when accounting for cell-cycle phase, rapidly cycling cells showed increased expression of genes associated with proliferation (*NME1*, *CCND2*, *FBXO6*) while slowly cycling cells expressed transcriptional elements associated with innateness and quiescence (*LITAF*, *ZFP36L2*) (Galloway et al., 2016; Gutierrez-Arcelus et al., 2019). ZFP36L2 plays a vital role in maintaining and re-establishing quiescence in B cells after expansion and has also been shown to inhibit lymphomagenesis by antagonizing Myc (Galloway et al., 2016). Conversely, increased expression of *NFKBIA* (IkB $\alpha$ ) in slowly cycling cells combined with increased expression of *ASB2* and *TESC* in rapidly cycling cells hints at NF- $\kappa$ B activation within the latter population (Wu et al., 2018; You et al., 2014). In both CD4<sup>+</sup> and CD8<sup>+</sup> T cells, homeostatic proliferation is dependent on NF- $\kappa$ B activation (Schmidt-Suprian et al., 2004). NF- $\kappa$ B activation has been linked to the induction of matrix metalloproteinases (MMP) and thus the potential to regulate cell migration (Bond et al., 2001; Li et al., 2012). Although no MMP genes were differentially expressed in our dataset, a number of genes associated with

actin-binding and migration/adhesion were upregulated in slowly (S100A4, S100A6, *TIMP1*) and rapidly cycling cells (ASB2, *TMSB10*, *ITGB7*, *CAPG*, *COTL1*). *TIMP1* is an inhibitor of MMPs, while *S100A4* (calvasculin) and *S100A6* (calcyclin) are recruited to the F-actin rich immune synapse (IS) and are associated with LFA-1 expression (Arpino et al., 2015; Urlaub et al., 2017). Conversely, ASB2 targets filamins, which are important for organizing F-actin, for degradation while *TMSB10* binds and sequesters G-actin, effectively inhibiting actin polymerization (Heuzé et al., 2008; Yu et al., 1993). *CAPG* further contributes by capping the barbed ends of actin filaments to prevent further polymerization, while *COTL1* has been shown to localize at the IS in T cells and associates with F-actin (Kim et al., 2014; Silacci et al., 2004). Considering the role actin plays in immune synapse formation, conjugate formation, and cytotoxic granule transportation to the surface (Carisey et al., 2018), modified actin polymerization during intense proliferation could impact target cell responsiveness. Although IL-15 stimulation induced granzyme B production in a proliferation dependent manner, this did not translate into increased target cell killing. Hence, further studies looking at the role of actin organization and immune synapse formation in rapidly cycling cells is warranted to delineate the mechanisms allowing switching from a proliferative to a cytotoxic and target-seeking mode.

In mice, IL-15-induced, mTOR activation-dependent metabolic reprogramming has been observed (Donnelly et al., 2014; Marçais et al., 2014; Nandagopal et al., 2014). Stimulation induced aerobic glycolysis allows for increased rates of biosynthesis and glycolytic flux that are essential for rapidly proliferating cells (Assmann and Finlay, 2016). Two metabolic enzymes, *GAPDH* and *ENTPD1* (CD39), were upregulated in rapidly versus slowly cycling cells. CD39 is an ectoenzyme whose immunosuppressive role has mainly been investigated in tumor-infiltrating monocytes and T cells. CD39 expression on myeloid-derived suppressor cells is a downstream effect of mTOR-mediated HIF1 $\alpha$  activation, and CD39<sup>+</sup>CD8<sup>+</sup> T cells exhibit an exhausted phenotype characterized by reduced cytokine production that could be stress-induced (Canale et al., 2018; Li et al., 2017). Similarly, stress signals can induce re-distribution of GAPDH within the cell (Bai et al., 2015). Within the nucleus, GAPDH can regulate transcription and translation by binding to RNA and DNA (Castello et al., 2015; Kim and Dang, 2005; Yu and Li, 2017). In highly glycolytic T cells, GAPDH can induce translation of IFN $\gamma$  and IL-2 by dissociating from Rheb that then activates mTORC1 (Kim and Dang, 2005; Kim, 2018). In line with increased cellular stress, apoptosis-related genes were increased within rapidly cycling cells (*BCL7C*, *CEBD*, *HSPD1*, *FBXO6*) while *KLRF1* (NKp80) was increased in slowly cycling cells. Apoptosis controls NK cell expansion but not proliferation (Huntington et al., 2007; Min-Oo et al., 2014). Hence increased apoptosis within rapidly cycling cells could account for the low overall fold change observed despite rapid proliferation. At resting state, NK cells possess intracellular stores of the NKp80 ligand AICL and express NKp80 on their surface. Cytokine stimulation induced internalization of the receptor and surface expression of the ligand, sensitizing activated NK cells to fratricide by NKp80-expressing NK cells (Klimosch et al., 2013). Evidently, increased metabolic activity and cellular stress levels in rapidly

cycling cells could contribute to the loss of functionality we observe in this population.

Our results provide insights into how IL-15-induced intra-lineage plasticity effectively maintains phenotypically and functionally diverse NK cell repertoires within individuals during homeostasis. Exploring the role of intra-lineage plasticity in tissue-specific niches or in conditions of perturbed homeostasis, such as during treatment with IL-15 agonists or post stem cell transplantation, will further our understanding of NK-cell-mediated anti-leukemia effects. Similarly, further studies into the mechanism behind the donor intrinsic mTOR activation would provide valuable information for modulating the proliferative capacity of specific subsets of NK cells, for example, in the case of adoptive NK cell therapy where donor selection is limited, and cellular expansion is a necessity.

## STAR★METHODS

Detailed methods are provided in the online version of this paper and include the following:

- KEY RESOURCES TABLE
- LEAD CONTACT AND MATERIALS AVAILABILITY
- EXPERIMENTAL MODEL AND SUBJECT DETAILS
- METHOD DETAILS
  - Cell Processing
  - Flow Cytometry
  - Flow Cytometry Analysis
  - Functional Assays
  - Inhibitor Experiments
  - Single-Cell RNA Sequencing
  - Bioinformatics Analysis
- QUANTIFICATION AND STATISTICAL ANALYSIS
- DATA AND CODE AVAILABILITY

## SUPPLEMENTAL INFORMATION

Supplemental Information can be found online at <https://doi.org/10.1016/j.celrep.2019.10.058>.

## ACKNOWLEDGMENTS

This work was supported by grants from the Swedish Research Council, the Swedish Children's Cancer Society, the Swedish Cancer Society, the Tobias Foundation, the Karolinska Institutet, the Norwegian Cancer Society, the Norwegian Research Council, the South-Eastern Norway Regional Health Authority, and the KG Jebsen Center for Cancer Immunotherapy. B.J. was funded by a Mildred Scheel postdoctoral scholarship from the Dr. Mildred Scheel Foundation for Cancer Research of the German Cancer Aid Organization.

## AUTHOR CONTRIBUTIONS

A.P. and B.J. conducted experiments. A.P. analyzed the data. S.L. performed RNA sequencing and generated the libraries. H.N. analyzed the RNA-seq data. E.H.A. generated the t-SNE plots. J.P.G., T.C., E.S., and K.-J.M. provided scientific input. A.P. wrote the original draft. E.S. and K.-J.M. designed research and reviewed and edited the manuscript.

## DECLARATION OF INTERESTS

K.-J.M. is a scientific advisor and consultant at FATE Therapeutics. J.P.G. is an employee at FATE Therapeutics. The current work is non-related to the research activities at FATE and has been conducted without any financial support from FATE Therapeutics.

Received: February 20, 2019

Revised: August 28, 2019

Accepted: October 14, 2019

Published: November 19, 2019

## REFERENCES

- Ali, A.K., Nandagopal, N., and Lee, S.-H. (2015). IL-15-PI3K-AKT-mTOR: a critical pathway in the life journey of natural killer cells. *Front. Immunol.* **6**, 355.
- Anton, O.M., Vielkind, S., Peterson, M.E., Tagaya, Y., and Long, E.O. (2015). NK Cell Proliferation Induced by IL-15 Transpresentation Is Negatively Regulated by Inhibitory Receptors. *J. Immunol.* **195**, 4810–4821.
- Arpino, V., Brock, M., and Gill, S.E. (2015). The role of TIMPs in regulation of extracellular matrix proteolysis. *Matrix Biol.* **44–46**, 247–254.
- Assmann, N., and Finlay, D.K. (2016). Metabolic regulation of immune responses: therapeutic opportunities. *J. Clin. Invest.* **126**, 2031–2039.
- Bai, A., Moss, A., Rothweiler, S., Serena Longhi, M., Wu, Y., Junger, W.G., and Robson, S.C. (2015). NADH oxidase-dependent CD39 expression by CD8(+) T cells modulates interferon gamma responses via generation of adenosine. *Nat. Commun.* **6**, 8819.
- Bézat, V., Liu, L.L., Malmberg, J.A., Ivarsson, M.A., Sohlberg, E., Björklund, A.T., Retière, C., Sverremark-Ekström, E., Traherne, J., Ljungman, P., et al. (2013). NK cell responses to cytomegalovirus infection lead to stable imprints in the human KIR repertoire and involve activating KIRs. *Blood* **121**, 2678–2688.
- Björkström, N.K., Riese, P., Heuts, F., Andersson, S., Fauriat, C., Ivarsson, M.A., Björklund, A.T., Flodström-Tullberg, M., Michaëlsson, J., Rottenberg, M.E., et al. (2010). Expression patterns of NKG2A, KIR, and CD57 define a process of CD56dim NK-cell differentiation uncoupled from NK-cell education. *Blood* **116**, 3853–3864.
- Bond, M., Chase, A.J., Baker, A.H., and Newby, A.C. (2001). Inhibition of transcription factor NF-κappaB reduces matrix metalloproteinase-1, -3 and -9 production by vascular smooth muscle cells. *Cardiovasc. Res.* **50**, 556–565.
- Boyman, O., Létourneau, S., Krieg, C., and Sprent, J. (2009). Homeostatic proliferation and survival of naïve and memory T cells. *Eur. J. Immunol.* **39**, 2088–2094.
- Canale, F.P., Ramello, M.C., Núñez, N., Araujo Furlan, C.L., Bossio, S.N., Gorosito Serrán, M., Tosello Boari, J., Del Castillo, A., Ledesma, M., Sedlik, C., et al. (2018). CD39 expression defines cell exhaustion in tumor-infiltrating CD8+ T cells. *Cancer Res.* **78**, 115–128.
- Carisey, A.F., Mace, E.M., Saeed, M.B., Davis, D.M., and Orange, J.S. (2018). Nanoscale Dynamism of Actin Enables Secretory Function in Cytolytic Cells. *Curr. Biol.* **28**, 489–502.
- Castello, A., Hentze, M.W., and Preiss, T. (2015). Metabolic Enzymes Enjoying New Partnerships as RNA-Binding Proteins. *Trends Endocrinol. Metab.* **26**, 746–757.
- Cichocki, F., Sitnicka, E., and Bryceson, Y.T. (2014). NK cell development and function—plasticity and redundancy unleashed. *Semin. Immunol.* **26**, 114–126.
- Collins, P.L., Celli, M., Porter, S.I., Li, S., Gurewitz, G.L., Hong, H.S., Johnson, R.P., Oltz, E.M., and Colonna, M. (2019). Gene Regulatory Programs Confering Phenotypic Identities to Human NK Cells. *Cell* **176**, 348–360.
- Colonna, M. (2018). Innate Lymphoid Cells: Diversity, Plasticity, and Unique Functions in Immunity. *Immunity* **48**, 1104–1117.
- Della Chiesa, M., Falco, M., Podestà, M., Locatelli, F., Moretta, L., Frassoni, F., and Moretta, A. (2012). Phenotypic and functional heterogeneity of human NK cells developing after umbilical cord blood transplantation: a role for human cytomegalovirus? *Blood* **119**, 399–410.

- Donnelly, R.P., Loftus, R.M., Keating, S.E., Liou, K.T., Biron, C.A., Gardiner, C.M., and Finlay, D.K. (2014). mTORC1-dependent metabolic reprogramming is a prerequisite for NK cell effector function. *J. Immunol.* 193, 4477–4484.
- Foley, B., Cooley, S., Verneris, M.R., Pitt, M., Curtsinger, J., Luo, X., Lopez-Vergès, S., Lanier, L.L., Weisdorf, D., and Miller, J.S. (2012). Cytomegalovirus reactivation after allogeneic transplantation promotes a lasting increase in educated NKG2C+ natural killer cells with potent function. *Blood* 119, 2665–2674.
- Galloway, A., Saveliev, A., Łukasiak, S., Hodson, D.J., Bolland, D., Balmanno, K., Ahlfors, H., Monzón-Casanova, E., Mannurita, S.C., Bell, L.S., et al. (2016). RNA-binding proteins ZFP36L1 and ZFP36L2 promote cell quiescence. *Science* 352, 453–459.
- Gao, Y., Souza-Fonseca-Guimaraes, F., Bald, T., Ng, S.S., Young, A., Ngiow, S.F., Rautela, J., Straube, J., Waddell, N., Blake, S.J., et al. (2017). Tumor immunoevasion by the conversion of effector NK cells into type 1 innate lymphoid cells. *Nat. Immunol.* 18, 1004–1015.
- Goldrath, A.W., Bogatzki, L.Y., and Bevan, M.J. (2000). Naive T cells transiently acquire a memory-like phenotype during homeostasis-driven proliferation. *J. Exp. Med.* 192, 557–564.
- Goodridge, J.P., Önfelt, B., and Malmberg, K.-J. (2015). Newtonian cell interactions shape natural killer cell education. *Immunol. Rev.* 267, 197–213.
- Gordon, S.M., Chaix, J., Rupp, L.J., Wu, J., Madera, S., Sun, J.C., Lindsten, T., and Reiner, S.L. (2012). The transcription factors T-bet and Eomes control key checkpoints of natural killer cell maturation. *Immunity* 36, 55–67.
- Gumá, M., Angulo, A., Vilches, C., Gómez-Lozano, N., Malats, N., and López-Botet, M. (2004). Imprint of human cytomegalovirus infection on the NK cell receptor repertoire. *Blood* 104, 3664–3671.
- Gutierrez-Arcelus, M., Teslovich, N., Mola, A.R., Polidoro, R.B., Nathan, A., Kim, H., Hannes, S., Slowikowski, K., Watts, G.F.M., Korsunsky, I., et al. (2019). Lymphocyte innateness defined by transcriptional states reflects a balance between proliferation and effector functions. *Nat. Commun.* 10, 687.
- Hafemeister, C., and Satija, R. (2019). Normalization and variance stabilization of single-cell RNA-seq data using regularized negative binomial regression. *bioRxiv*. <https://doi.org/10.1101/576827>.
- Hesslein, D.G.T., Palacios, E.H., Sun, J.C., Beilke, J.N., Watson, S.R., Weiss, A., and Lanier, L.L. (2011). Differential requirements for CD45 in NK-cell function reveal distinct roles for Syk-family kinases. *Blood* 117, 3087–3095.
- Heuzé, M.L., Lamsoul, I., Baldassarre, M., Lad, Y., Lévéque, S., Razinina, Z., Moog-Lutz, C., Calderwood, D.A., and Lutz, P.G. (2008). ASB2 targets filamins A and B to proteasomal degradation. *Blood* 112, 5130–5140.
- Horowitz, A., Strauss-Albee, D.M., Leipold, M., Kubo, J., Nemat-Gorgani, N., Dogan, O.C., Dekker, C.L., Mackey, S., Maecker, H., Swan, G.E., et al. (2013). Genetic and environmental determinants of human NK cell diversity revealed by mass cytometry. *Sci. Transl. Med.* 5, 208ra145.
- Horowitz, A., Djaoud, Z., Nemat-Gorgani, N., Blokhuis, J., Hilton, H.G., Béziat, V., Malmberg, K.-J., Norman, P.J., Guethlein, L.A., and Parham, P. (2016). Class I HLA haplotypes form two schools that educate NK cells in different ways. *Sci. Immunol.* 1, 1–14.
- Huntington, N.D., Puthalakath, H., Gunn, P., Naik, E., Michalak, E.M., Smyth, M.J., Tabarias, H., Degli-Esposti, M.A., Dewson, G., Willis, S.N., et al. (2007). Interleukin 15-mediated survival of natural killer cells is determined by interactions among Bim, Noxa and Mcl-1. *Nat. Immunol.* 8, 856–863.
- Keating, S.E., Zaiatz-Bittencourt, V., Loftus, R.M., Keane, C., Brennan, K., Finlay, D.K., and Gardiner, C.M. (2016). Metabolic Reprogramming Supports IFN- $\gamma$  Production by CD56bright NK Cells. *J. Immunol.* 196, 2552–2560.
- Kim, J.W., and Dang, C.V. (2005). Multifaceted roles of glycolytic enzymes. *Trends Biochem. Sci.* 30, 142–150.
- Kim, J. (2018). Regulation of Immune Cell Functions by Metabolic Reprogramming. *J. Immunol. Res.* 2018, 8605471.
- Kim, J., Shapiro, M.J., Bamidele, A.O., Gurel, P., Thapa, P., Higgs, H.N., Hedin, K.E., Shapiro, V.S., and Billadeau, D.D. (2014). Coactosin-like 1 antagonizes cofilin to promote lamellipodial protrusion at the immune synapse. *PLoS One* 9, e85090.
- Klimosch, S.N., Bartel, Y., Wiemann, S., and Steinle, A. (2013). Genetically coupled receptor-ligand pair NKp80-AICL enables autonomous control of human NK cell responses. *Blood* 122, 2380–2389.
- Krzywinska, E., Cornillon, A., Allende-Vega, N., Vo, D.N., Rene, C., Lu, Z.Y., Pasero, C., Olive, D., Fegueux, N., Ceballos, P., et al. (2016). CD45 isoform profile identifies natural killer (NK) subsets with differential activity. *PLoS ONE* 11, e0150434.
- Laurent, P., Jolivel, V., Manicki, P., Chiu, L., Contin-Bordes, C., Truchetet, M.E., and Pradeu, T. (2017). Immune-mediated repair: A matter of plasticity. *Front. Immunol.* 8, 454.
- Li, Y.F., Xu, X.B., Chen, X.H., Wei, G., He, B., and Wang, J.D. (2012). The nuclear factor- $\kappa$ B pathway is involved in matrix metalloproteinase-9 expression in RU486-induced endometrium breakdown in mice. *Hum. Reprod.* 27, 2096–2106.
- Li, J., Wang, L., Chen, X., Li, L., Li, Y., Ping, Y., Huang, L., Yue, D., Zhang, Z., Wang, F., et al. (2017). CD39/CD73 upregulation on myeloid-derived suppressor cells via TGF- $\beta$ -mTOR-HIF-1 signaling in patients with non-small cell lung cancer. *Oncol Immunol* 6, e1320011.
- Lin, J.X., Du, N., Li, P., Kazemian, M., Gebregiorgis, T., Spolski, R., and Leonard, W.J. (2017). Critical functions for STAT5 trimers in the maturation and survival of natural killer cells. *Nat. Commun.* 8, 1320.
- Liu, L.L., Pfefferle, A., Yi Sheng, V.O., Björklund, A.T., Béziat, V., Goodridge, J.P., and Malmberg, K.-J. (2015). Harnessing adaptive natural killer cells in cancer immunotherapy. *Mol. Oncol.* 9, 1904–1917.
- Lopez-Vergès, S., Milush, J.M., Schwartz, B.S., Pando, M.J., Jarjoura, J., York, V.A., Houchins, J.P., Miller, S., Kang, S.M., Norris, P.J., et al. (2011). Expansion of a unique CD57<sup>+</sup>NKG2Chi natural killer cell subset during acute human cytomegalovirus infection. *Proc. Natl. Acad. Sci. USA* 108, 14725–14732.
- Lutz, C.T., Karapetyan, A., Al-Attar, A., Shelton, B.J., Holt, K.J., Tucker, J.H., and Presnell, S.R. (2011). Human NK cells proliferate and die in vivo more rapidly than T cells in healthy young and elderly adults. *J. Immunol.* 186, 4590–4598.
- Marçais, A., Cherfils-Vicini, J., Viant, C., Degouve, S., Viel, S., Fenis, A., Rabiloud, J., Mayol, K., Tavares, A., Bienvenu, J., et al. (2014). The metabolic checkpoint kinase mTOR is essential for IL-15 signaling during the development and activation of NK cells. *Nat. Immunol.* 15, 749–757.
- Marçais, A., Marotel, M., Degouve, S., Koenig, A., Fauteux-Daniel, S., Drouillard, A., Schlums, H., Viel, S., Besson, L., Allatif, O., et al. (2017). High mTOR activity is a hallmark of reactive natural killer cells and amplifies early signaling through activating receptors. *eLife* 6, 1–21.
- Mauri, M., Elli, T., Caviglia, G., Ubaldi, G., and Azzi, M. (2017). RAWGraphs: A Visualisation Platform to Create Open Outputs. In Proceedings of the 12th Biannual Conference on Italian SIGCHI Chapter.
- Min, B. (2018). Spontaneous T cell proliferation: A physiologic process to create and maintain homeostatic balance and diversity of the immune system. *Front. Immunol.* 9, 547.
- Min-Oo, G., Bezman, N.A., Madera, S., Sun, J.C., and Lanier, L.L. (2014). Pro-apoptotic Bim regulates antigen-specific NK cell contraction and the generation of the memory NK cell pool after cytomegalovirus infection. *J. Exp. Med.* 211, 1289–1296.
- Nandagopal, N., Ali, A.K., Komal, A.K., and Lee, S.H. (2014). The critical role of IL-15-PI3K-mTOR pathway in natural killer cell effector functions. *Front. Immunol.* 5, 187.
- Poli, A., Michel, T., Thérésine, M., Andrès, E., Hentges, F., and Zimmer, J. (2009). CD56bright natural killer (NK) cells: an important NK cell subset. *Immunology* 126, 458–465.
- Ranson, T., Vossenrich, C.A., Corcuff, E., Richard, O., Müller, W., and Di Santo, J.P. (2003a). IL-15 is an essential mediator of peripheral NK-cell homeostasis. *Blood* 101, 4887–4893.
- Ranson, T., Vossenrich, C.A.J., Corcuff, E., Richard, O., Laloux, V., Lehuen, A., and Di Santo, J.P. (2003b). IL-15 availability conditions homeostasis of peripheral natural killer T cells. *Proc. Natl. Acad. Sci. USA* 100, 2663–2668.

- Santourlidis, S., Trompeter, H.-I., Weinhold, S., Eisermann, B., Meyer, K.L., Wernet, P., and Uhrberg, M. (2002). Crucial role of DNA methylation in determination of clonally distributed killer cell Ig-like receptor expression patterns in NK cells. *J. Immunol.* **169**, 4253–4261.
- Schlums, H., Cichocki, F., Tesi, B., Theorell, J., Beziat, V., Holmes, T.D., Han, H., Chiang, S.C., Foley, B., Mattsson, K., et al. (2015). Cytomegalovirus infection drives adaptive epigenetic diversification of NK cells with altered signaling and effector function. *Immunity* **42**, 443–456.
- Schmidt-Supplian, M., Tian, J., Ji, H., Terhorst, C., Bhan, A.K., Grant, E.P., Pasparakis, M., Casola, S., Coyle, A.J., and Rajewsky, K. (2004). IκB kinase 2 deficiency in T cells leads to defects in priming, B cell help, germinal center reactions, and homeostatic expansion. *J. Immunol.* **173**, 1612–1619.
- Silacci, P., Mazzolai, L., Gauci, C., Stergiopoulos, N., Yin, H.L., and Hayoz, D. (2004). Gelsolin superfamily proteins: key regulators of cellular functions. *Cell. Mol. Life Sci.* **61**, 2614–2623.
- Soliman, G.A. (2013). The role of mechanistic target of rapamycin (mTOR) complexes signaling in the immune responses. *Nutrients* **5**, 2231–2257.
- Stegmann, K.A., Björkström, N.K., Veber, H., Ciesek, S., Riese, P., Wiegand, J., Hadem, J., Suneetha, P.V., Jaroszewicz, J., Wang, C., et al. (2010). Interferon- $\alpha$ -induced TRAIL on natural killer cells is associated with control of hepatitis C virus infection. *Gastroenterology* **138**, 1885–1897.
- Streltsova, M.A., Erokhina, S.A., Kanevskiy, L.M., Lee, D.A., Telford, W.G., Sapozhnikov, A.M., and Kovalenko, E.I. (2018). Analysis of NK cell clones obtained using interleukin-2 and gene-modified K562 cells revealed the ability of “senescent” NK cells to lose CD57 expression and start expressing NKG2A. *PLoS ONE* **13**, e0208469.
- Stuart, T., Butler, A., Hoffman, P., Hafemeister, C., Iii, W.M.M., Stoeckius, M., Smibert, P., and Satija, R. (2018). Comprehensive integration of single cell data. *bioRxiv*. <https://doi.org/10.1101/460147>.
- Sun, J.C., Beilke, J.N., and Lanier, L.L. (2009). Adaptive immune features of natural killer cells. *Nature* **457**, 557–561.
- Takeda, K., Cretney, E., Hayakawa, Y., Ota, T., Akiba, H., Ogasawara, K., Yagita, H., Kinoshita, K., Okumura, K., and Smyth, M.J. (2005). TRAIL identifies immature natural killer cells in newborn mice and adult mouse liver. *Blood* **105**, 2082–2089.
- Tirosh, I., Izar, B., Prakadan, S.M., Wadsworth, M.H., 2nd, Treacy, D., Trombetta, J.J., Rotem, A., Rodman, C., Lian, C., Murphy, G., et al. (2016). Dissecting the multicellular ecosystem of metastatic melanoma by single-cell RNA-seq. *Science* **352**, 189–196.
- Urlaub, D., Höfer, K., Müller, M.-L., and Watzl, C. (2017). LFA-1 Activation in NK Cells and Their Subsets: Influence of Receptors, Maturation, and Cytokine Stimulation. *J. Immunol.* **198**, 1944–1951.
- van Dijk, D., Sharma, R., Nainys, J., Yim, K., Kathail, P., Carr, A.J., Burdziak, C., Moon, K.R., Chaffer, C.L., Pattabiraman, D., et al. (2018). Recovering Gene Interactions from Single-Cell Data Using Data Diffusion. *Cell* **174**, 716–729.e27.
- Viel, S., Marçais, A., Guimaraes, F.S., Loftus, R., Rabilloud, J., Grau, M., Degouve, S., Djebali, S., Sanlaville, A., Charrier, E., et al. (2016). TGF- $\beta$  inhibits the activation and functions of NK cells by repressing the mTOR pathway. *Sci. Signal.* **9**, ra19.
- Viel, S., Besson, L., Marotel, M., Walzer, T., and Marçais, A. (2017). Regulation of mTOR, Metabolic Fitness, and Effector Functions by Cytokines in Natural Killer Cells. *Cancers (Basel)* **9**, 1–12.
- Vivier, E., Raulet, D.H., Moretta, A., Caligiuri, M.A., Zitvogel, L., Lanier, L.L., Yokoyama, W.M., and Ugolini, S. (2011). Innate or Adaptive Immunity? The Example of Natural Killer Cells. *Science* **331**, 44–49.
- Wang, F., Meng, M., Mo, B., Yang, Y., Ji, Y., Huang, P., Lai, W., Pan, X., You, T., Luo, H., et al. (2018). Crosstalks between mTORC1 and mTORC2 variate cytokine signaling to control NK maturation and effector function. *Nat. Commun.* **9**, 4874.
- Wu, W., Nie, L., Zhang, L., and Li, Y. (2018). The notch pathway promotes NF- $\kappa$ B activation through Asb2 in T cell acute lymphoblastic leukemia cells. *Cell. Mol. Biol. Lett.* **23**, 37.
- Yang, C., Tsaih, S.W., Lemke, A., Flister, M.J., Thakar, M.S., and Malarkannan, S. (2018). mTORC1 and mTORC2 differentially promote natural killer cell development. *eLife* **7**, 1–25.
- You, D.J., Park, C.R., Lee, H.B., Moon, M.J., Kang, J.H., Lee, C., Oh, S.H., Ahn, C., Seong, J.Y., and Hwang, J.I. (2014). A splicing variant of NME1 negatively regulates NF- $\kappa$ B signaling and inhibits cancer metastasis by interacting with IKK $\beta$ . *J. Biol. Chem.* **289**, 17709–17720.
- Yu, X., and Li, S. (2017). Non-metabolic functions of glycolytic enzymes in tumorigenesis. *Oncogene* **36**, 2629–2636.
- Yu, F.X., Lin, S.C., Morrison-Bogorad, M., Atkinson, M.A.L., and Yin, H.L. (1993). Thymosin beta 10 and thymosin beta 4 are both actin monomer sequestering proteins. *J. Biol. Chem.* **268**, 502–509.
- Zhang, M., Wen, B., Anton, O.M., Yao, Z., Dubois, S., Ju, W., Sato, N., DiLillo, D.J., Bamford, R.N., Ravetch, J.V., and Waldmann, T.A. (2018). IL-15 enhanced antibody-dependent cellular cytotoxicity mediated by NK cells and macrophages. *Proc. Natl. Acad. Sci. USA* **115**, E10915–E10924.

**STAR★METHODS****KEY RESOURCES TABLE**

REAGENT or RESOURCE	SOURCE	IDENTIFIER
<b>Antibodies</b>		
CD107a – AF700	Beckton Dickinson	H4A3
CD107a – PE-Cy5	Beckton Dickinson	H4A3
CD14 – V500	Beckton Dickinson	MφP9
CD19 – V500	Beckton Dickinson	HIB19
CD3 – V500	Beckton Dickinson	UCHT1
CD57 – BV605	Beckton Dickinson	NK-1
Granzyme B – AF700	Beckton Dickinson	GB11
CD16 purified	Beckton Dickinson	3G8
CD158a, h – PE-Cy7	Beckman Coulter	EB6B
CD158b1/b2, j – PE-Cy5.5	Beckman Coulter	GL183
CD159a – APC-AF750	Beckman Coulter	Z199
CD3 – PE-Cy5	Beckman Coulter	UCHT1
CD56 – ECD	Beckman Coulter	N901
CD158e1 – APC	Biolegend	DX9
CD158e-1 – Biotin	Biolegend	DX9
CD16 – BV785	Biolegend	3G8
CD57 – FITC	Biolegend	HNK-1
IFN $\gamma$ -BV785	Biolegend	4S.B3
CD158a – APC	Miltenyi Biotec	REA284
CD158a – APC Vio770	Miltenyi Biotec	REA284
CD158e/k – Biotin	Miltenyi Biotec	5.133
CD158e/k – PE	Miltenyi Biotec	5.133
CD159a – PE Vio770	Miltenyi Biotec	REA110
CD159c – PE	Miltenyi Biotec	REA205
Ki-67 – PE Vio770	Miltenyi Biotec	REA183
KIR2D – Biotin	Miltenyi Biotec	NKVFS1
KIR2D – PE	Miltenyi Biotec	NKVFS1
TNF $\alpha$ -APC	eBioscience	MAb11
p-S6 ribosomal protein (S235/236) – PE	Cell Signaling Technologies	D57.2.2E
KIR2DL3 – FITC	R&D Systems	180701
Streptavidin – QD705	Life Technologies	Q10161MP
Caspase-3 – FITC	Abcam	ab65613
<b>Chemicals, Peptides, and Recombinant Proteins</b>		
Recombinant Human IL-15 GMP Protein, CF	R&D	247-GMP-025
Rapamycin	Sigma	8781-200UL
Torin-1	Apexbio	A8312
Ficoll-Hypaque Plus	GE Healthcare	GE17-1440-02
L-Glutamine	Ge Healthcare	82024-258
Protein transport inhibitor (containing Monensin)	BD Bioscience	554724
Protein transport inhibitor (containing Brefeldin A)	BD Bioscience	555029
<b>Critical Commercial Assays</b>		
LIVE/DEAD Fixable Aqua Dead Cell Stain kit, 405 nM	Life Technologies	L34965
CellTrace Violet Cell Proliferation kit, for flow cytometry	Life Technologies	C34557

(Continued on next page)

**Continued**

REAGENT or RESOURCE	SOURCE	IDENTIFIER
Intracellular Fixation & Permeabilization buffer set	eBioscience	88-8824-00
NK cell isolation kit	Miltenyi Biotec	130-092-657
CellTrace CFSE Cell proliferation kit, for flow cytometry	Life Technologies	C34554
Chromium Single Cell 3' Library & Gel Bead Kit v2	Chromium Controller System, 10X Genomics	PN-120237
Deposited Data		
Single-cell RNA sequencing dataset	European Genome-phenome Archive	EGAS00001003946
Software and Algorithms		
R	N/A	<a href="https://www.r-project.org">https://www.r-project.org</a>
FlowJo version 9	TreeStar Inc	<a href="https://www.flowjo.com">https://www.flowjo.com</a>
Prism 6	GraphPad	<a href="https://www.graphpad.com/scientific-software/prism/">https://www.graphpad.com/scientific-software/prism/</a>
Ingenuity Pathway Analysis	QIAGEN	<a href="https://www.qiagen.com/de/products/informatics-and-data/interpretation-content-databases/ingenuity-pathway-analysis/#orderinginformation">https://www.qiagen.com/de/products/informatics-and-data/interpretation-content-databases/ingenuity-pathway-analysis/#orderinginformation</a>
RAW graphs	Mauri et al., 2017	<a href="https://rawgraphs.io/">https://rawgraphs.io/</a>
Other		
RPMI medium, without glutamine	GE Healthcare	SH30086.FS
Stem Cell Growth Medium (SCGM)	CellGenix	20802-0500
Human serum	Sigma	H3667-100mL

**LEAD CONTACT AND MATERIALS AVAILABILITY**

This study did not generate new reagents. Further information and requests for resources and reagents should be directed to and will be fulfilled by the Lead Contact, Karl-Johan Malmberg ([kalle.malmberg@ki.se](mailto:kalle.malmberg@ki.se)).

**EXPERIMENTAL MODEL AND SUBJECT DETAILS**

The majority of donors used in this study were obtained either from the Karolinska University Hospital or Oslo University Hospital blood bank (anonymous donors) and experiments were performed with freshly isolated NK cells. Informed consent was obtained, and the study was approved by the regional ethics committee in Norway (scRNA-seq) and Sweden (2016/1415-32, 2018/2485). For Figures 3A–3C, 4F, S3, and S4, frozen cells from previously genotyped healthy blood donors were used (9M/10F, age 30–78). Two of these donors had an adaptive NK cell population. In Figures 2B and 2D–2H, NK cells were isolated from whole blood taken monthly over a 3-month period from the same 6 healthy volunteers (3M/3F, age 23–31). KIR HLA-Ligand typing was performed using the OLERUP SSP kit (Lot# 39Y). For the single-cell RNA sequencing, one donor had an adaptive NK cell population. Information regarding the number of donors represented by each figure can be found in the figure legend. For functional readouts, K562 cells were used as target cells.

**METHOD DETAILS****Cell Processing**

Using density gradient centrifugation, peripheral mononuclear cells (PBMC) were isolated from healthy blood donors (Karolinska University Hospital, Oslo University Hospital) with informed consent and as approved by the regional ethics committee (2016/1415-32, 2018/2482). NK cells were purified using magnetic-activated cell sorting (MACS) and labeled with 1 μM cell proliferation dye. NK cells were resuspended in Stem Cell Growth Medium (SCGM) (10% human serum, 2mM L-glutamine, 5ng/mL IL-15) at 1,5x10<sup>6</sup> cells/mL and cultured in 96U-bottom wells (200 μL) at 37°C/5% CO<sub>2</sub>. IL-15 was replenished daily and 100 μL medium was refreshed on day 3. Visualization plots (Figures 1B, 1C, 1E, and 3B) were created using RAW Graphs (Mauri et al., 2017).

**Flow Cytometry**

Cells were harvested and stained in 96 V-bottom plates for surface antigens and viability, fixed/permeabilized and stained intracellularly. Samples were acquired on an LSR-Fortessa (355, 405, 488, 561, 639 nm lasers). Sorting experiments were performed at 4°C

on a FACS Aria Fusion (405, 488, 561, 633 nm lasers) and a FACS Aria II (405, 488, 561, 640 nm lasers). Data were analyzed in FlowJo version 9 (TreeStar, Inc.).

### Flow Cytometry Analysis

To minimize variation for daily readouts over the course of one week, CS&T beads (BD Bioscience) and application settings in FACS DIVA were used to eliminate daily fluctuations in the LSR-Fortessa. Additional controls included usage of a reference sample, consisting of a buffy coat frozen in small aliquots which was thawed and stained for each experimental readout. Values were then adjusted based on the reference values which were normalized over the days.

Fold change of pS6 expression on a particular day was calculated by comparing the observed expression to baseline expression at day 0. Expansion index, the overall fold expansion of the culture, was calculated based on the CTV dilution using the Proliferation tool in FlowJo.

t-distributed Stochastic Neighbor Embedding (t-SNE) analysis was performed using the Rtsne package (<http://cran.r-project.org/web/packages/Rtsne/index.html>) in R version 3.1.0. Events from one representative donor were divided into generations by manual gating on CTV in FlowJo version 9. Then, 20,000 events were randomly sampled from each generation and data were pooled and arcsinh transformed using cofactor 150. The t-SNE calculations were based on the markers NKG2A, CD57, CD16, KIR2DL1, KIR2DL1/S1, KIR2DL3, KIR2DL2/S2/L3, KIR3DL1, Granzyme B and pS6. Plots were generated using FlowJo or the ggplot2 R package (<http://cran.r-project.org/web/packages/ggplot2/index.html>) and red borders were added using Photoshop CS6 (Adobe). “nKIR” values were generated based on manual gating of KIR2DL1, KIR2DL3 and KIR3DL1 in FlowJo.

Self-KIR is based on HLA-C – KIR2D interaction whereby C1/C1 or C2/C2 donors were used and only single self-KIR positive cells were included in the analysis. Education via KIR3DL1-Bw4 was not taken into account, and therefore we cannot exclude that a sub-population of NK cell was educated via this interaction in [Figure 4F](#).

### Functional Assays

Cells were harvested, counted, and seeded at a 1:1 effector:target ratio in complete RPMI medium (10% Fetal calf serum, 2mM L-glutamine). Natural cytotoxicity and antibody-dependent cellular cytotoxicity (ADCC) assays were performed with K562 and P815, pre-incubated with purified CD16 antibody, respectively. The cells were incubated (4h) in the presence of brefeldin A (1:1000 concentration), monensin (1:1500 concentration) and CD107a antibody. Post incubation, normal surface/intracellular staining was performed. For the flow cytometry based killing assays, NK cells were seeded at a 1:1 effector:target ratio with K562 in complete RPMI medium with Caspase 3- FITC in a 96V-bottom plate. The plate was centrifuged at 300 rpm (3 min) and incubated at 37°C (4h). Post incubation, the cells were surface stained and fixed.

### Inhibitor Experiments

After 4 days of stimulation (5ng/mL IL-15), cells were treated with DMSO, Rapamycin (25, 50 nM) or Torin1 (125, 250 nM) in the presence of continued IL-15 (48h).

### Single-Cell RNA Sequencing

PBMCs from healthy blood donors were screened for KIR education. NK cells were isolated on an AutoMACS (DepleteS program, Miltenyi Biotec), labeled with 1 μM CTV and rested overnight in complete RPMI medium. Two populations (CD56<sup>dim</sup>NKG2A<sup>+</sup>non-self-/selfKIR<sup>-</sup>CD57<sup>+</sup> & CD56<sup>dim</sup>NKG2A<sup>-/+</sup>non-selfKIR<sup>-</sup>selfKIR<sup>+</sup>CD57<sup>+</sup>NKG2C<sup>-/+</sup>) were sorted for single-cell RNA sequencing while CD56<sup>dim</sup> NKG2A<sup>-</sup> non-selfKIR<sup>-</sup> selfKIR<sup>+</sup> CD57<sup>+</sup> cells were sorted for culture ([Figure S5](#)). Sorting was performed at 4°C using a FACS Aria II. Sorted cells were cultured in SCGM (10% human serum, 2mM L-glutamine, 5ng/mL IL-15) in 96U-bottom wells (200 μL) at 37°C/ 5% CO<sub>2</sub>. IL-15 was replenished daily and 100 μL medium was refreshed on day 3. After 6 days, NK cells were stained and FACS sorted based on cell division (CTV) into slowly (CD56<sup>+</sup> Generation 0-1) and rapidly cycling (CD56<sup>+</sup> Generation 2+).

For single-cell RNA sequencing, 12,000 cells were sorted (4°C) for each sample. Cells were washed (PBS + 0.05% BSA) and counted. 10,000 cells were resuspended in 35 μL PBS + 0.05% BSA and immediately processed at the Genomics Core Facility (Oslo University Hospital) using the Chromium Single Cell 3' Library & Gel Bead Kit v2 (Chromium Controller System, 10X Genomics). The sequencing libraries were generated following the recommended protocol. Sequencing was performed on a NextSeq500 (Illumina) with 5~% PhiX as spike-in. Sequencing raw data were converted into fastq files by running the Illumina's bcl2fastq v2.

### Bioinformatics Analysis

The processed 10x files were analyzed in R using Seurat version 3.0 ([Hafemeister and Satija, 2019; Stuart et al., 2018](#)). The four IL-15 samples (day 6) consisted of two samples from each of the two donors. Quality control was performed to remove potential outliers or doublets based on the number of counts, the number of features and the percentage of mitochondrial genes in the cells. 7207 cells of the IL-15 samples passed the quality control thresholds. The samples from the same donors were merged and normalized using SCTransform. Subsequently the samples were integrated across donors by using the data integration method implemented in Seurat version 3.0 ([Hafemeister and Satija, 2019; Stuart et al., 2018](#)). Linear dimensionality reduction was performed using PCA, where the number of principle components (PCs) to use for the downstream analysis was determined by JackStraw and Elbow plots. Non-linear dimensionality reduction was subsequently performed on these PCs using UMAP.

A cell cycle score for each cell was calculated using the expression of a list of cell cycle markers that is loaded with Seurat ([Tirosh et al., 2016](#)). By applying the CellCycleScoring function in Seurat, the cells were assigned to the different cell cycle phases (G1 – 3502 cells, S – 2413 cells, G2/M – 1292 cells). The cells assigned to the G1 phase were used to identify differentially expressed genes between the rapidly and slowly cycling cells. By comparing the two cell populations within this cell cycle phase and using the Wilcoxon Rank Sum test with a log fold change threshold of 0.25 to identify the differentially expressed genes between these two groups, 63 marker genes were identified. The expression of these genes in the two populations were plotted on a heatmap ordered by the fold change. Clustering was performed using the graph based (Louvain) clustering method in Seurat with various resolutions.

The baseline samples consisted of two samples from each of the two donors where one donor had an adaptive subset. QC was performed as stated above, where 7908 cells in the baseline samples passed the quality control thresholds. Merging, normalization, data integration, dimensionality reduction, clustering, and cell cycle score computations were performed in the same way as for the IL-15 samples.

To integrate the baseline and the IL-15 (day 6) samples, the cells assigned to the G1 cell cycle phase were integrated with the baseline samples using Seurat data integration. Dimensionality reduction, clustering, and cell cycle score computations were performed as described above. The data imputation method MAGIC ([van Dijk et al., 2018](#)) was used to impute the gene expression of the 63 marker genes identified for rapidly/slowly cycling cells. These imputed expression levels were plotted onto the UMAP embedding.

## QUANTIFICATION AND STATISTICAL ANALYSIS

Significance was calculated using a Wilcoxon signed rank test or, when comparing more than 3 groups, a Friedman test followed by Dunn's multiple comparisons test. Linear regression analysis was performed followed by a Spearman r test to determine significance for correlations. p values: \* < 0.05, \*\* < 0.01, \*\*\* < 0.001, \*\*\*\* < 0.0001. GraphPad Prism 6 software was used for statistical analysis and the exact test used for each figure panel can be found in the corresponding figure legend. For the scRNA-seq analysis, Seurat version 3 was used for analysis and further information can be found in the method details section.

## DATA AND CODE AVAILABILITY

The single-cell RNA sequencing data generated during this study are available at the European Genome-phenome Archive (EGA), accession number EGA: EGAS00001003946.

**Supplemental Information**

**Intra-lineage Plasticity and Functional  
Reprogramming Maintain Natural Killer  
Cell Repertoire Diversity**

**Aline Pfefferle, Benedikt Jacobs, Herman Netskar, Eivind Heggernes Ask, Susanne Lorenz, Trevor Clancy, Jodie P. Goodridge, Ebba Sohlberg, and Karl-Johan Malmberg**

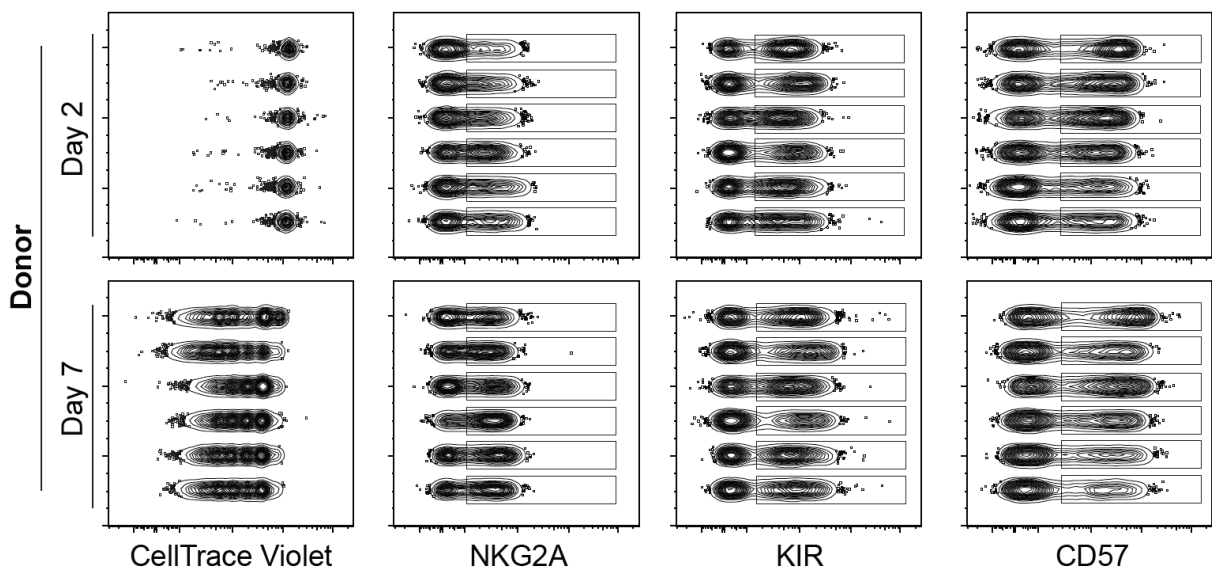


**Figure S1. Inter-donor variation in response to IL-15 stimulation (Related to Figure 1)**

Concatenated FACS plots showing CTV dilution and surface expression of NKG2A, KIR and CD57 of the total NK cell population on day 2 and day 7 in IL-15 stimulated cells. n = 6 from one representative experiment.

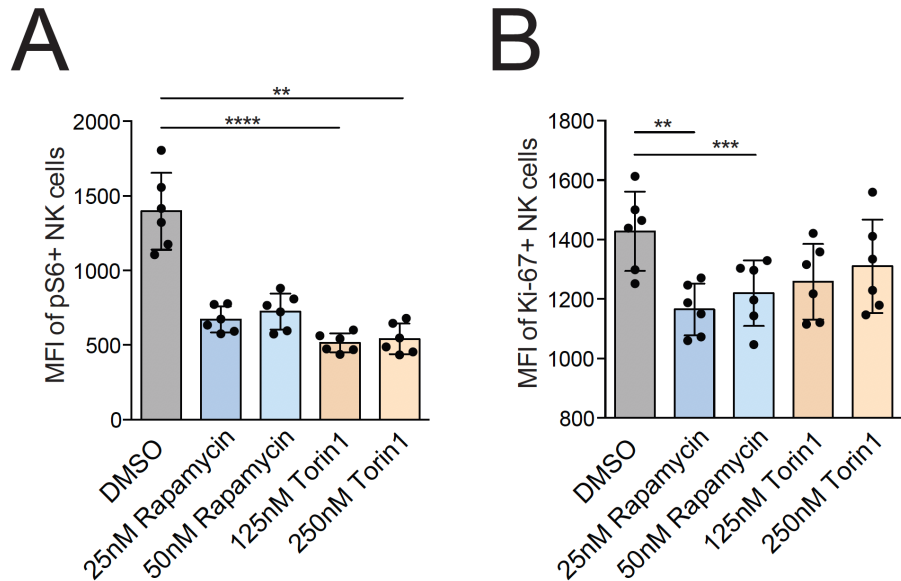


**Figure S2. mTOR inhibition in proliferating NK cells (Related to Figure 2)**

(A and B) Mean fluorescent intensity of pS6 (A) and Ki-67 (B) on day 6 in IL-15 stimulated NK cells treated with DMSO, 25nM Rapamycin, 50nM Rapamycin, 125nM Torin-1 or 250nM Torin-1 for 48h prior to readout. n = 6 from one representative experiment. Data are represented as mean (SD). Significance was calculated using a Friedman test followed by Dunn's multiple comparisons test (A-B). p-values: \* < 0.05, \*\* < 0.01, \*\*\* < 0.001, \*\*\*\* < 0.0001.

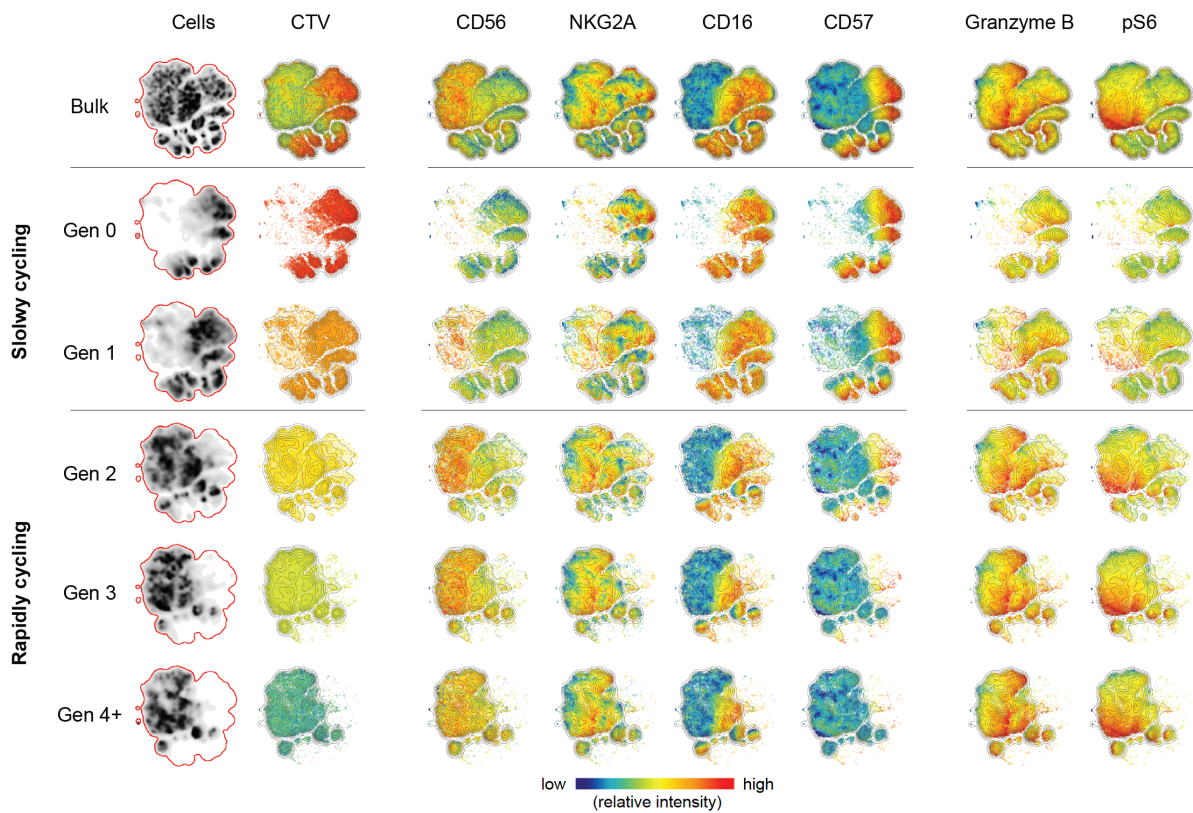


**Figure S3. Phenotype of proliferating NK cells observed at the generation level (Related to Figure 3)**

t-SNE plots showing the relative intensity of CD56, NKG2A, CD16, CD57, Granzyme B and pS6 expression in the total NK cell population and gated on individual generations using CTV dilution in one representative donor on day 5. n = 1 from one representative experiment.

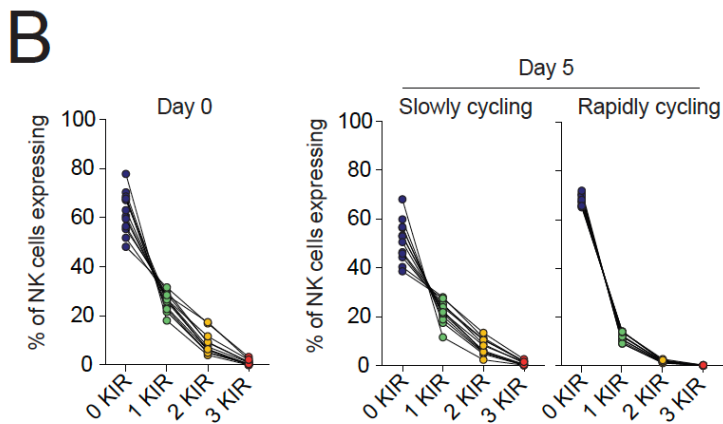
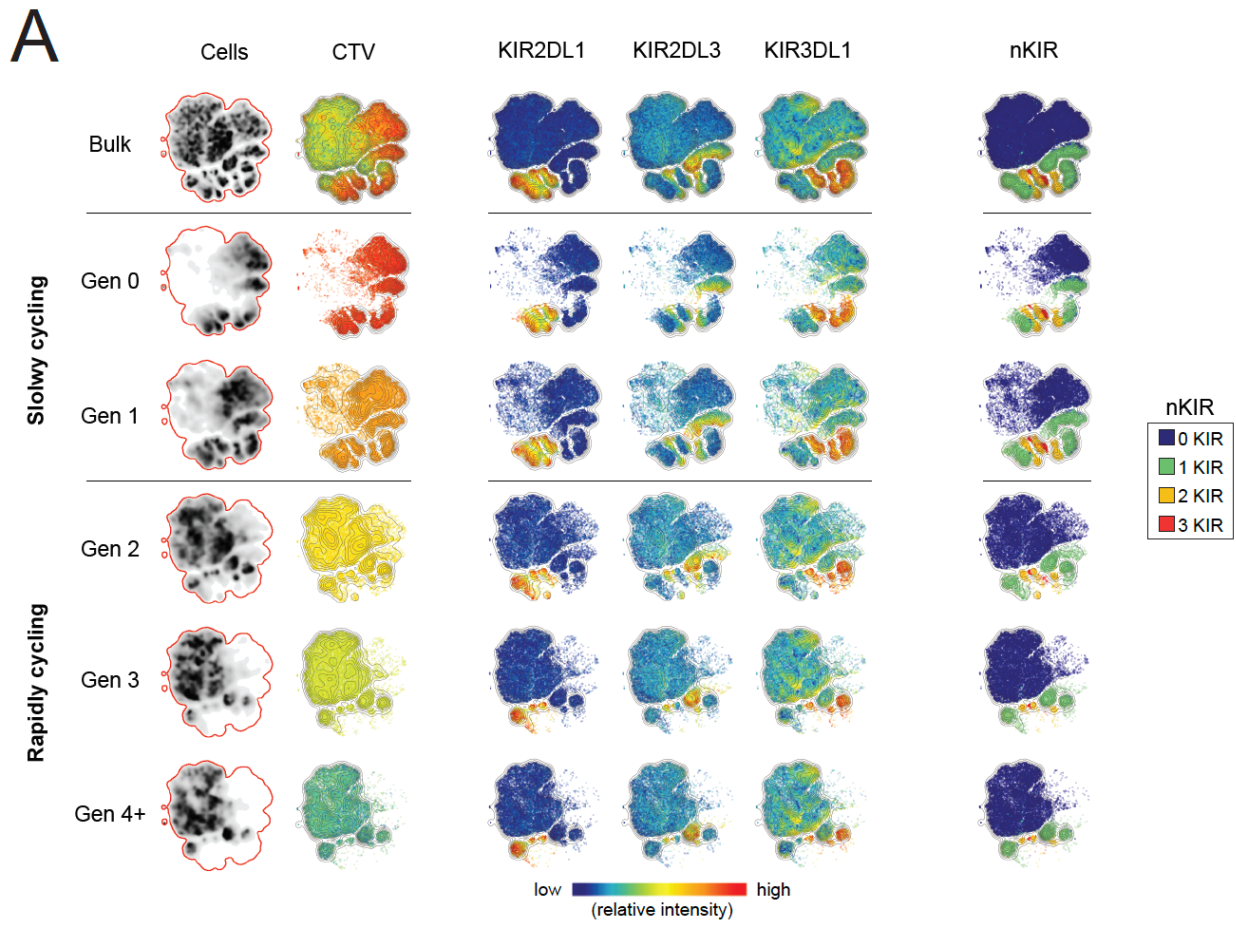


**Figure S4. KIR repertoires of proliferating NK cells at the generation level (Related to Figure 4)**

**(A)** t-SNE plots showing the relative intensity of KIR2DL1, KIR2DL3 and KIR3DL1 expression, as well as the number of KIR (nKIR) expressed per cell, in the total NK cell population and gated on individual generations using CTV dilutions in one representative donor on day 5. **(B)** The frequency of NK cells expressing 0-3 KIR at baseline and within slowly (Generation 0-1) and rapidly cycling (Generation 2+) cells on day 5.  $n = 1-12$  from 2 independent experiments. In **(B)** 3 longitudinal samples from 4 donors each were analyzed with  $>1$  year in between sampling.

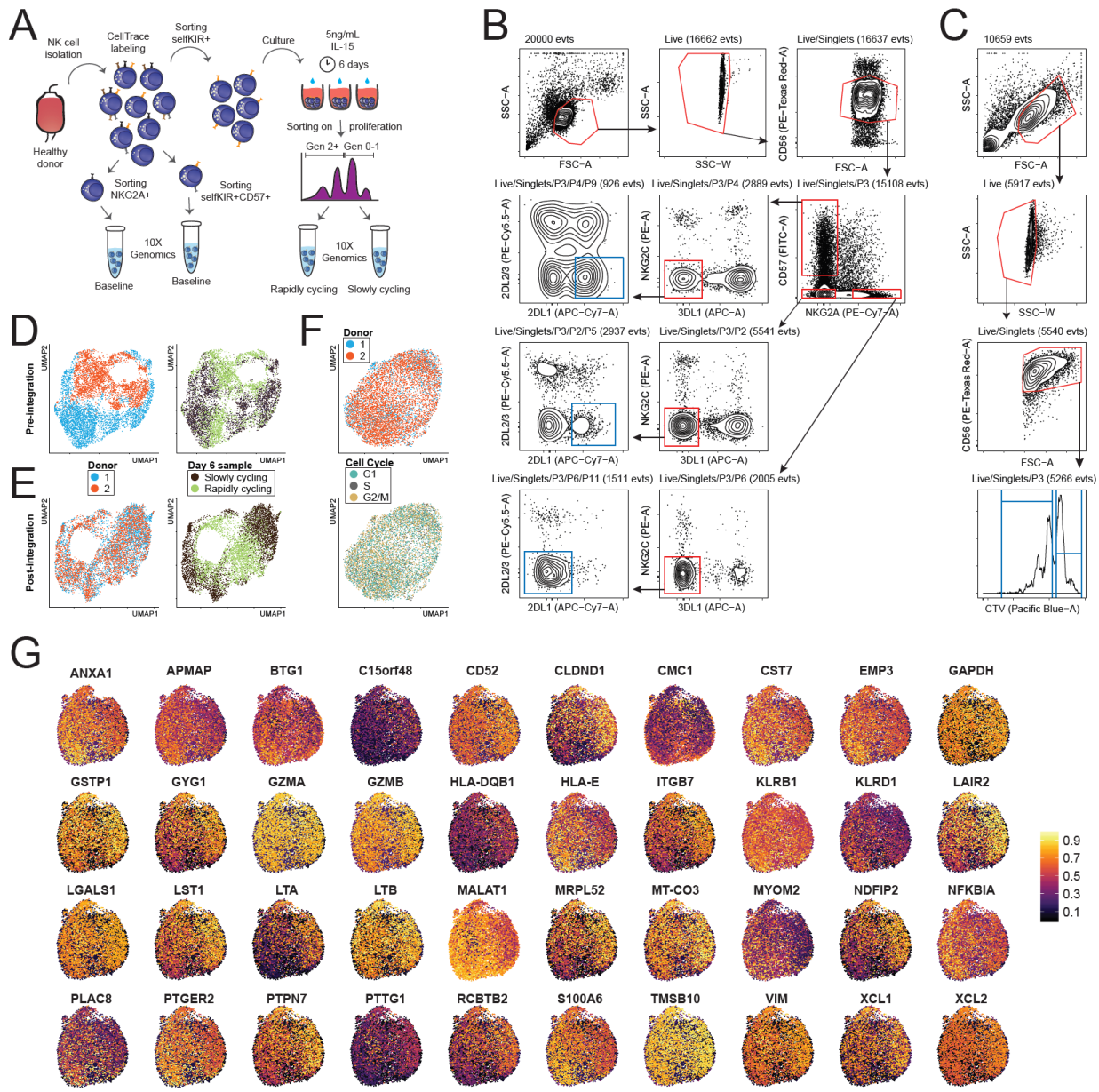


**Figure S5. Design and analysis of single-cell RNA sequencing experiments (Related to Figure 5)**

(A) Graphical methodology outline for upstream sample preparation before single-cell RNA sequencing using the 10x Genomics platform. (B) The gating strategy used to sort distinct CD56<sup>dim</sup> NK cell populations at baseline from healthy blood donors. NKG2A<sup>+</sup>KIR<sup>-</sup>CD57<sup>+</sup> and NKG2A<sup>-/-</sup>selfKIR<sup>+</sup>CD57<sup>+</sup>NKG2C<sup>-/-</sup> subsets were sorted for single-cell RNA sequencing. NKG2A<sup>-</sup>selfKIR<sup>+</sup>CD57<sup>+</sup> cells were sorted and placed in culture with IL-15 for 6 days to induce proliferation. Blue gates denote the sorted populations. (C) The gating strategy used to re-sort the previously sorted NKG2A<sup>-</sup>selfKIR<sup>+</sup>CD57<sup>+</sup> into slowly (generation 0-1) and rapidly (generation 2+) cycling cells based on CellTrace Violet dilution. Blue gates denote the sorted populations. (D and E) UMAP embedding of the four day 6 scRNA-seq samples depicting donor and sample information for each cell before (D) and after (E) data integration. (F) UMAP embedding of the four baseline scRNA-seq samples depicting donor information and cell cycle phase for each cell after data integration. (G) Imputed gene expression of a selection of the 63 DEGs plotted onto the UMAP embedding of baseline and day 6 samples. n = 4-8 from 4 independent experiments.

---

**63 differentially expressed genes at day 6**

<b>↑ slowly cycling</b>	<b>↑ rapidly cycling</b>	
FGFBP2	PTTG1	ITGB7
CCL5	PTPN7	NDFIP2
MALAT1	BCL7C	GZMB
S100A4	TMSB10	TNFSF10
KLRF1	GZMA	GZMK
FCGR3A	XCL2	HLA-DQB1
LITAF	CEBDP	MRPL52
KLRD1	ENTPD1	KLRC1
CST7	MT-CO3	LGALS1
CMC1	HSPD1	RCBTB2
BTG1	FBXO6	XCL1
PTPRC	LAIR2	LTA
TIMP1	CCND2	C15orf48
KLRB1	GSTP1	CAPG
ZFP36L2	ASB2	COTL1
MYOM2	CLDND1	
PLAC8	NME1	
HLA-E	GYG1	
ANXA1	GAPDH	
PTGER2	TESC	
S100A6	LST1	
EMP3	VIM	
NFKBIA	LTB	
APMAP	CD52	

**Table S1. Differentially expressed genes between slowly and rapidly cycling cells (Related to Figure 5)**

Genes that were differentially expressed between slowly and rapidly cycling cells day 6 within the G1 phase of the cell cycle. The 63 genes are ordered from highest to lowest fold.